



Published in final edited form as:

Exp Eye Res. 2021 May ; 206: 108541. doi:10.1016/j.exer.2021.108541.

Role of the superior salivatory nucleus in parasympathetic control of choroidal blood flow and in maintenance of retinal health

Chunyan Li^a, Malinda E.C. Fitzgerald^{a,b,c}, Nobel Del Mar^a, Hongbing Wang^a, Corey Haughey^a, Marcia G. Honig^a, Anton Reiner^{a,b,*}

^aDepartment of Anatomy and Neurobiology, USA

^bDepartment of Ophthalmology, University of Tennessee, 855 Monroe Ave, Memphis, TN, 38163, USA

^cDepartment of Biology, Christian Brothers University, Memphis, TN, 38104, USA

Abstract

The vasodilatory pterygopalatine ganglion (PPG) innervation of the choroid is under the control of preganglionic input from the superior salivatory nucleus (SSN), the parasympathetic portion of the facial motor nucleus. We sought to confirm that choroidal SSN drives a choroid-wide vasodilation and determine if such control is important for retinal health. To the former end, we found, using transscleral laser Doppler flowmetry, that electrical activation of choroidal SSN significantly increased choroidal blood flow (ChBF), at a variety of choroidal sites that included more posterior as well as more anterior ones. We further found that the increases in ChBF were significantly reduced by inhibition of neuronal nitric oxide synthase (nNOS), thus implicating nitrergic PPG terminals in the SSN-elicited ChBF increases. To evaluate the role of parasympathetic control of ChBF in maintaining retinal health, some rats received unilateral lesions of SSN, and were evaluated functionally and histologically. In eyes ipsilateral to choroidal SSN destruction, we found that the flash-evoked scotopic electroretinogram a-wave and b-wave peak amplitudes were both significantly reduced by 10 weeks post lesion. Choroidal baroregulation was evaluated in some of these rats, and found to be impaired in the low systemic arterial blood pressure (ABP) range where vasodilation normally serves to maintain stable ChBF. In retina ipsilateral to SSN destruction, the abundance of Müller cell processes immunolabeled for glial fibrillary acidic protein (GFAP) and GFAP message were significantly upregulated. Our studies indicate that the SSN-PPG circuit mediates parasympathetic vasodilation of choroid, which appears to contribute to

This is an open access article under the CC BY-NC-ND license (<http://creativecommons.org/licenses/by-nc-nd/4.0/>).

*Corresponding author. Department of Anatomy & Neurobiology University of Tennessee Health Science Center, 855 Monroe Ave, Memphis, TN, 38163, USA. areiner@uthsc.edu (A. Reiner).

Author contributions

Chunyan Li performed choroidal blood flow studies, analyzed their results, analyzed choroidal innervation patterns, and assisted in the preparation of the manuscript. Malinda E.C. Fitzgerald performed choroidal blood flow and ERG studies and analyzed their results, performed brain lesion studies and the immunohistochemical evaluation of their results, and assisted in the preparation of the manuscript. Nobel Del Mar assisted in the choroidal blood flow and ERG studies. Corey Haughey assisted in the immunohistochemical evaluation of the retinal effects of the brain lesions. Marcia G. Honig assisted in the analysis of choroidal innervation patterns. Anton Reiner planned the studies, analyzed their results, and prepared the manuscript and its illustrations.

Declarations of competing interest

None.

ChBF baroregulation during low ABP. Our results further indicate that impairment in this adaptive mechanism results in retinal dysfunction and pathology within months of the ChBF disturbance, indicating its importance for retinal health.

Keywords

Choroidal blood flow (ChBF); Superior salivatory nucleus (SSN); Retinal degeneration; Autonomic; Parasympathetic

1. Introduction

The retina has two vascular supplies: the retinal vessels within the retina itself, and the choroidal vessels external to Bruch's membrane and the retinal pigment epithelium (Alm, 1992). The retinal vessels provide blood supply to the inner two-thirds of the retina, while the outer retina is avascular and nourished from the choroid (Alm, 1992). Flow through the choroid is, however, much more substantial than that to the inner retina, and accordingly, the choroid provides 65–85% of the oxygen to the retina, with variation among species (Alm, 1992; Alm and Bill, 1973). Diminishing choroidal blood flow by occluding one or more the posterior ciliary arteries feeding choroid (Hayreh, 2004; Loeffler et al., 1994) or occluding a vortex vein (Collier, 1967) rapidly destroys the outer retina, and outer retinal hypoxia yields rapid RPE and photoreceptor dysfunction and/or loss (Braun and Linsenmeier, 1995; Linsenmeier et al., 1983; Linsenmeier and Steinberg, 1986; Yancey and Linsenmeier, 1988, 1989). In light of this, the reductions in ChBF seen in aging and various retinal diseases, such as systemic hypertension, diabetic retinopathy and age-related macular degeneration (Fitzgerald et al., 2001; Grunwald et al., 1998a, 1998b, 2005; Ito et al., 2001; Metelitsina et al., 2008; Pournaras et al., 2006) are of interest, as they raise the possibility that these ChBF reductions contribute to the retinal declines associated with these conditions.

Although ChBF was once thought to respond passively to changes in perfusion pressure, more recent studies have shown that ChBF remains stable over a systemic blood pressure range of about 35% above and below basal (Kiel and Shepherd, 1992; Li et al., 2018; Lovasik et al., 2003; Reiner et al., 2003, 2011), with neural mechanisms apparently involved in the compensation (Kiel, 1999; Li et al., 2010, 2015, 2018, 2010; Reiner et al., 2010, 2018). When blood pressure is low, choroidal blood vessels dilate to maintain flow, and when blood pressure is high, choroidal blood vessels constrict, preventing overperfusion, tissue edema, and oxidative injury (Reiner et al., 2018). Neurogenic choroidal vasodilation is mediated by parasympathetic innervation of choroidal vessels, and neurogenic choroidal vasoconstriction is accomplished by sympathetic innervation (Reiner et al., 2018). Several features of the central and peripheral circuitry subserving parasympathetic contributions to choroidal baroregulation have been characterized. The parasympathetic pterygopalatine ganglion (PPG) innervates orbital vessels feeding the choroid and intrachoroidal vessels (Reiner et al., 2012, 2018). The PPG input to choroid and to choroidal feeder vessels employs the vasodilators nitric oxide (NO) and vasoactive intestinal polypeptide (VIP), and as a result these vessels are densely coated with nerve fibers containing neuronal nitric oxide synthase (which synthesizes NO in neurons) and VIP (Reiner et al., 2012, 2018; Stone et al., 1987).

The preganglionic neurons regulating the PPG reside in the superior salivatory nucleus (SSN), the autonomic component of the facial motor complex in the hindbrain (Cuthbertson et al., 2003). In prior studies in rats, we found that a major input to choroidal SSN arose from the part of the nucleus of the solitary tract (NTS) of the medulla that receives baroreceptive input and is responsive to blood pressure signals (Li et al, 2010, 2015). In more recent studies, we found that activation of this part of NTS increases ChBF in the ipsilateral eye, and that the peripheral PPG terminals mediating this effect appear to use NO as a vasodilator (Li et al., 2016b). These results are consistent with the view that the NTS input to the choroidal part of SSN enables the adaptive parasympathetic regulation of ChBF during systemic hypotension. Only one study, however, has directly examined the influence of SSN on ChBF (Steinle et al., 2000), and that study suggested that SSN only influenced ChBF in the anterior superior sector of the eye. Moreover, that study did not examine the importance of SSN control of ChBF for retinal health. In the present study, we examined the regional extent of SSN influence on ChBF and the impact of impaired SSN control of ChBF on retinal health.

2. Materials and methods

2.1. Experimental overview

Adult male Sprague-Dawley (SD) rats (290–380 g; from Harlan, Indianapolis, IN) were used in the present studies. To confirm that SSN drives a choroid-wide nitric oxide (NO) - mediated vasodilation, we activated the choroidal part of SSN by electrical stimulation while monitoring ChBF from both anterior and posterior sites along the superior surface of the eye to assess if the effect on ChBF was pervasive, and evaluated the ability of neuronal nitric oxide synthase (NOS) inhibition to diminish the evoked vasodilation. To further assess the extent of PPG influence on the choroid, we examined the regional distribution of its input to choroid. An additional set of rats were used to examine the effect of unilateral choroidal SSN destruction on retinal function as evaluated by the flash-evoked scotopic ERG, and on retinal health as determined by immunolabeling of Müller cell processes for glial fibrillary acidic protein (GFAP), and qPCR assessment of retinal GFAP levels. Prior to being sacrificed, ChBF baroregulation was assessed in some of the rats used in ERG analysis. All experiments were in compliance with the ARVO statement on the Use of Animals in Ophthalmic and Vision Research, and with NIH and institutional guidelines.

2.2. Studies of effects of SSN stimulation on choroidal blood flow

2.2.1. Choroidal blood flow surgical preparation—Rats were anesthetized for surgery by intraperitoneal (ip) injection of 0.1 ml/100 g body weight of a ketamine/xylazine mixture (87/13 mg/kg), with supplemental doses (0.05–0.07 ml of ketamine/xylazine mixture) every 25–30 min. To prepare the surgical sites, the dorsum of the head and ventrum of the hind legs were shaved. To measure systemic arterial blood pressure (ABP), the femoral artery was cannulated with PE-50 polyethylene tubing pre-soaked with heparinized saline (40 units/ml). A Digi-Med Blood Pressure Analyzer™ (BPA-100, Micro-Med, Inc., Louisville, KY) was used to measure arterial blood pressure (ABP) via a pressure transducer connected to the femoral artery cannula. The femoral vein was cannulated for administration of N^ω-propyl-L-arginine (NPA, 1–2 mg/kg, Tocris Bioscience), a selective nNOS inhibitor

(Cooper et al., 2000; Zhang et al., 1997), or N^{ω} -nitro-L-arginine methyl ester (LNAME), an inhibitor of both nNOS and endothelial NOS (Zagvazdin et al, 1996a, 1996b). The rats were then positioned in a stereotaxic device, and a pulse oximeter clipped on the tail to measure systemic blood oxygen saturation. Body temperature was maintained at 37 °C with a Harvard heating blanket and rectal thermoprobe.

To prepare the eye for transscleral measurement of ChBF, fascia and the parts of the Harderian gland overlying the superior aspect of the right eye were removed. The tip of a laser Doppler probe connected to a LASERFLO BPM² blood perfusion monitor (Vasamedics; Eden Prairie, MN or BPM 403A; TSI Incorporated; St. Paul, MN) was positioned 1–3 mm above the sclera with a micromanipulator. Measurements of ChBF were made from the vascular bed beneath the sclera at the three sites shown in Fig. 1: 1) just lateral to the superior rectus muscle at its insertion; 2) in the gap between the superior and medial rectus muscles, just anterior to the equator of the superior part of the eye; and 3) in the gap between the superior and medial rectus muscles, just posterior to the equator of the superior part of the eye. A small amount of Aquasonic ultrasound gel (Parker Laboratories, Inc.; Fairfield, NJ) or 33% glycerol – 0.1 M sodium phosphate buffer (PB) was used in the interface between the probe tip and sclera to mitigate tissue drying. For placement of a stimulating electrode, the skin over the skull was retracted and a hole drilled through bone overlying SSN. The coordinates for choroidal SSN from the rat brain atlas of (Paxinos and Watson, 2009) were: –10.5 mm behind Bregma, –2.2 mm lateral to Bregma, and –7.8 mm below the pial surface.

2.2.2. Choroidal blood flow measurement and choroidal SSN stimulation—As shown and discussed in our prior studies, laser Doppler flowmetry can be used to obtain reliable relative measures of ChBF, choroidal blood volume (ChBVol) and choroidal blood velocity (ChBVel) (Fitzgerald et al, 1990, 1996, 2001, 2005; Li et al, 2016b, 2018; Reiner et al., 2010; Zagvazdin et al., 1996a). Although the LASERFLO BPM² nominally presents ChBF values in ml blood per min per 100 g tissue (ml/min/100g), ChBVol in 12,000 red blood cells per cubic millimeter of tissue (12,000 RBC/mm³), and ChBVel as 10 mm/s, because of uncertainties about how well choroidal tissue matches the assumptions of the algorithms used to derive these measures, ChBF is reported here as relative blood flow units, ChBVol as relative blood volume units, and ChBVel as relative blood velocity units, as in our prior studies. The output of our LASERFLO BPM² was exported to a ML880 PowerLab 16/30 data acquisition system (ADInstruments Inc., Colorado Springs, CO), and the digitized data were collected and analyzed using LabChart v7 Pro software (ADInstruments Inc.) installed on an iMac Apple computer. The data averaging window of the BPM² was set at 0.3 s, with the sampling rate on PowerLab set at 200 samples/s.

Microstimulation consisted of a 7 s train of 100 Hz, 0.5 ms duration negative current pulses delivered by a S48 stimulator (Grass Instrument Company, Quincy, MA) and PSIU6 stimulus isolation unit (Grass Instrument Company). Stimulation was performed with either an insulated, stainless steel electrode (5 M Ω ; Catlog # 572000; A-M Systems Inc., Sequim, WA), or a glass micropipette. Micropipettes were pulled from glass tubing (World Precision Instrument, 1B150F-4) with a PE-2 microelectrode puller (Narashige), and micropipettes with a tip diameter of 50–100 μ m used for stimulation. Micropipettes were filled with

artificial cerebral spinal fluid (ACSF) consisting of 126 mM NaCl, 26 mM NaHCO₃, 3 mM KCl, 1.25 mM NaH₂PO₄, 2 mM MgCl₂, 2 mM CaCl₂, and 20 mM glucose; pH 7.3, 310 mOsm, and a platinum wire was inserted. Current pulse amplitude for activating SSN was 5 μ A for metal electrodes, and a mean of 17.3 μ A for glass electrodes. Data presented here for each rat represent an average of 3–7 SSN stimulation trials. In some rats, we additionally studied the effects of nNOS inhibition on the ChBF increases elicited by SSN stimulation. In these studies, we administered NPA (1–2 mg/kg, Tocris Bioscience) or LNAME (10 mg/kg, Tocris Bioscience) intravenously (iv), and determined the effect on baseline ChBF and SSN-evoked increases in ChBF, ChBVol, ChBVel, and arterial blood pressure (ABP) over an additional 3–7 stimulation trials, and compared to SSN stimulation effects prior to inhibition. For any given rat, the stimulating current pulse amplitude used after NOS inhibition was the same as used before drug delivery.

2.2.3. Histological verification of stimulation sites—At the end of the ChBF recording session and while yet deeply anesthetized, rats were perfused transcardially with 150–200 ml sodium phosphate buffered saline (PBS, 0.9% sodium chloride dissolved in 0.01M PB), followed by 400–500 ml fixative of 4% paraformaldehyde prepared in 0.1 M sodium phosphate buffer (pH 7.4) with 0.1 M lysine and 0.01 M sodium periodate (the PLP fixative). Brains were removed and cryoprotected at 4 °C for at least 24 h in 20% sucrose - 10% glycerol - 0.138% sodium azide in 0.1 M sodium phosphate buffer. Brains were then frozen with dry ice, and coronal sections cut with a sliding microtome at 40 μ m and collected as 6 parallel series. We used four histological methods to confirm that electrode placement was within choroidal SSN: 1) analysis of the location of the electrode tip in choroidal SSN in cresyl violet-stained sections; 2) analysis of the location of the electrode tip in choroidal SSN in neuronal NOS (nNOS) immunostained sections; 3) analysis of the location of the electrode tip in choroidal SSN in choline acetyltransferase (ChAT) immunostained sections, and 4) analysis of the location of the electrode tip in choroidal SSN in cfos immunostained sections. Our immunolabeling and cresyl violet staining procedures have been described in detail in our previous publications (Deng et al., 2007; Li et al, 2010, 2016b). In some cases, two-color DAB labeling for cfos and nNOS (Li et al, 2015, 2016b) was used as in our prior studies to detect stimulation-activated (cfos+) neurons of choroidal SSN (nNOS+). The sections were examined with an Olympus BH-2 microscope with standard transmitted light. Images were captured using a Spot Idea™ camera and a Spot imaging software (Diagnostic Instruments, Inc.). Only rats with confirmed choroidal SSN stimulation sites are used here in the presentation of SSN stimulation data (Fig. 1).

2.2.4. Statistical analysis of SSN stimulation data—We analyzed the effects of choroidal SSN stimulation on ChBF, ChBVol, ChBVel, and ABP. For the time blocks prior to stimulation, we calculated the mean for ChBF, ChBVol, ChBVel, and ABP, which served as the baseline level for these parameters against which to evaluate stimulation effects. For analysis of the response to choroidal SSN activation, we compared the response during the 7 s of SSN stimulation to the response for that parameter in the 7 s prior to stimulation, using paired t-tests. For the nNOS inhibition studies, paired t-tests were used to compare choroidal SSN responses before nNOS inhibitor administration and after administration (during the time of drug efficacy). Regression analysis was used to evaluate the contributions of ABP,

ChBV_{ol} and ChBV_{el} changes to choroidal SSN stimulation-evoked ChBF changes. Group results are plotted as mean \pm SEM.

2.3. Studies of effects of choroidal SSN lesions

2.3.1. Choroidal SSN lesions—Unilateral electrolytic lesions of choroidal SSN were made in animals deeply anesthetized with ketamine/xylazine (87/13 mg/kg) by passing 1 mA anodal current for 15 s through a metal electrode placed in SSN, using stereotaxic methods as described above for stimulating electrode placement in choroidal SSN. Following a subcutaneous injection of lidocaine into the scalp, the skin and fascia overlying the skull were retracted, and a hole drilled in the skull overlying the lesion site, using the same coordinates as for stimulation studies. Following the lesion, the skin was sutured with wound clips, and the rat returned to its home cage after recovery from anesthesia. Wound clips were removed at 10–14 d after surgery.

2.3.2. Studies of effects of choroidal SSN destruction on the electroretinogram—Prior to the lesion and at about 4 and 10 weeks post lesion, the electroretinogram (ERG) was recorded with the Espion E² system from Diagnosys, with Espion V5 software (Version 5.0.52) running on Windows XP platform, as described previously (Li et al., 2018). Animals were dark adapted overnight, and anesthetized by ip injection of 0.1 ml/100g of a ketamine/xylazine mixture (87/13 mg/kg) prior to the ERG recording session. Each eye was dilated with 1% cyclopentolate hydrochloride Ophthalmic solution (NDC 17478-100-12 from Akorn). The dorsum of the head was shaved for placement of a reference electrode under the skin at the midpoint between orbits, and a ground electrode was inserted under the skin on the right hind foot. Reference and ground electrodes were disposable low-profile EEG needle electrodes (112-812-48 TP from Chalgren Enterprises, Inc. 380 Tomkins Ct. Gilroy, CA, 95020, USA). One drop of Methocel (2%, from OmniVision) was applied to the cornea of each eye when positioning gold ring electrodes (3 mm diameter Goldring; Roland Consult, Brandenburg, Germany), to promote conductivity and reduce impedance. A ColorDome Ganzfeld then was centered over the animal, and a series of seven light stimulus intensities were presented to the animal: 0.0001, 0.001, 0.01, 0.1, 1, 10, 758 cd s per meter squared (cd·s/m²). The lower light intensities test rod function and the last light intensity activates rods and cones. After the ERG recording, the rats were allowed to recover from anesthesia on a warming pad, and returned to their home cage. For analysis, the amplitudes and latencies of the a-wave and b-wave were measured for the averaged traces for each stimulus step with a custom Igor Pro (version 6.37) routine, and exported to Excel, with b-wave measured from baseline. One-way ANOVA with posthoc comparisons, using the Bonferroni correction for multiple comparisons, was performed using IBM SPSS Statistics (version 22) to evaluate ERG performance over time post lesion in rats with unilateral choroidal SSN lesions and in rats with lesions that missed choroidal SSN. Note that no effects on latency were observed, so our presentation focuses on amplitude.

2.3.3. Studies of the effects of choroidal SSN destruction on ChBF baroregulation—For six rats in which choroidal SSN was targeted for electrolytic destruction prior to ERG analysis, we examined ChBF baroregulation, measuring ChBF as

described above. For these studies, continuous ABP and ChBF signals were sampled at a rate of 200 samples/s, and analyzed with LabChart 7 Pro software. After about 30 min of baseline recording, blood was withdrawn (5 ml) to evaluate ChBF during low ABP for 10–15 min. Subsequently, LNAME in hepanized saline (50 mg/kg) was infused to assess ChBF baroregulation during high ABP, if needed, for an additional 30 min. For analysis, we selected 10 s blocks of ABP and ChBF for every minute of stable recording, and exported the values for each time block to Excel. To assess baroregulation, data for each rat were grouped into 5 mmHg bins, and all ABP values within a bin were averaged to calculate the mean ABP for that bin, as were the contemporaneous ChBF values for the samples in that same ABP bin range. Histological analysis revealed that 3 of the rats had choroidal SSN destruction and 3 did not. Accordingly, we could compare these two sets of rats to assess the impact of a choroidal SSN lesion on baroregulation during low systemic blood pressure.

2.3.4. Histology – perfusion and tissue harvest—Three-four months post surgery, rats with lesions targeting choroidal SSN used in the ERG studies or intended for immunohistochemical analysis of retina were deeply anesthetized with ketamine/xylazine (87/13 mg/kg), and perfused transcardially with 150–200 ml of 0.9% saline and 400–500 ml of paraformaldehyde prepared in 0.1 M sodium phosphate buffer (pH 7.4) with 0.1 M lysine and 0.01 M sodium periodate (PLP fixative). For the six rats used in assessing baroregulation, transcardial perfusion occurred immediately after the ChBF recording session. Eyes to be used for retinal immunolabeling were removed from the rats after perfusion, the cornea was incised with a sharp scalpel to create a flap, and PLP fixative was infused into the eye cup. The entire eye was then immersed in PLP for 2 h at 4 °C, the cornea and lens then removed, and the eye immersed in 20% sucrose prepared in 0.1 M sodium phosphate buffer (pH 7.4) with 0.02% sodium azide at 4 °C until cryosectioning for use in immunolabeling. Brains were evaluated for lesion accuracy using the same approach described above for assessing stimulation site accuracy.

2.3.5. Immunolabeling of retina—Eye cups were embedded for cryostat sectioning in OCT, frozen and sectioned across the horizontal meridian at 20 µm. The sections were collected onto pre-cleaned Superfrost®/Plus microscope slides as sectioned, dried on a slide warmer, and stored at –20 °C until processed for immunolabeling for retinal or choroidal markers, including glial fibrillary acidic protein (GFAP), VIP, VMAT2 (vesicular monoamine transporter 2), and nNOS (neuronal nitric oxide synthase). Labeling was visualized either by immunofluorescence or peroxidase anti-peroxidase (PAP) methods, as described in our prior studies (Kimble et al., 2006; Li et al, 2016b, 2018). Sections prepared by immunofluorescence were viewed and images captured using a Zeiss 710 confocal laser scanning microscope (CLSM). Sections prepared by the PAP method were analyzed and images captured using transmitted light microscopy. For analysis of GFAP immunolabeling in Müller cells as detected by the PAP method, retinal images were coded for blinded quantification of GFAP-immunolabeled retinal Müller cell processes, as described previously (Kimble et al., 2006). In brief, within a 200 µm window from two randomly sampled images from superior retina from each eye from each rat, each GFAP immunolabeled Müller cell process was scored on a 0–5 scale based on its penetrance into the retina from vitread to sclerad side and the total for all processed detected summed. The

score for each retina then reflected the abundance and penetrance of the GFAP immunolabeled Müller cell processes per 200 μm retinal length. Results for GFAP process scores were analyzed between SSN lesion rats and control rats (SSN misses and rats with no lesion) via unpaired t-tests.

2.3.6. qPCR of retina—To further assess the Müller cell response to choroidal SSN destruction, we used qPCR to measure GFAP expression in retina, using methods described in Honig et al. (2019). Control rats with either no lesion ($n = 3$) or a lesion that largely spared (94.0% intact) right choroidal SSN ($n = 2$), or rats with a lesion that largely destroyed (27.5% intact) right choroidal SSN ($n = 2$) were sacrificed, left and right retina separately dissected from each rat, and the tissue homogenized in TRIzol Reagent (Thermo Fisher Scientific, Waltham, MA). Chloroform was added to the homogenate, centrifuged, and the upper colorless phase transferred to a clean tube. Precipitation was with 100% isopropanol and linear acrylamide. Precipitate was washed with 75% ethanol and the final mRNA pellet was suspended in DEPC (diethylpyrocarbonate) treated water. For subsequent qPCR analysis, cDNA was generated using reverse transcription (RT) performed with the Transcriptor First Strand cDNA Synthesis Kit (Roche Applied Science, Mannheim, Germany), combining 100 ng of RNA with reaction buffer and enzyme mix, following manufacturer's directions. Primers and probes for GFAP are shown in Table 1.

3. Results

3.1. Effects of choroidal SSN stimulation on ChBF

3.1.1. Sampling of ChBF effects of choroidal SSN stimulation at different choroidal sites—We sampled ChBF responses to choroidal SSN stimulation via a metal electrode at two sites just anterior to the equator of the eye (one temporal to the insertion of the superior rectus and one nasal to the insertion of superior rectus), and a third site posterior to the equator and nasal to the superior rectus (Fig. 1). SSN stimulation with metal electrodes yielded significant choroidal blood flow increases at all three sites. For example, for rats assessed at the site temporal to the superior rectus (site 1 in Fig. 1), electrical activation of SSN with trains of 5 μA negative current pulses yielded mean ChBF increases that were 136.1% above prestimulation baseline ($p = 0.0162$), with peak increases that were 222.7% above baseline ($p = 0.0121$) (Fig. 2A). We found similar effects of SSN stimulation for rats assessed at the anterior nasal site (site 2 in Fig. 1). Electrical activation of SSN with trains of 5 μA negative current pulses yielded mean ChBF increases that were 165.4% above prestimulation baseline ($p = 0.0454$), with peak increases that were 330.2% above baseline ($p = 0.0048$) (Fig. 2B). Significant ChBF increases with 5 μA SSN stimulation were also observed for rats at the posterior nasal site (site 3 in Fig. 1), with mean increases being 127.6% above pre-stimulation baseline ($p = 0.0120$) and the peak increase being 239.8% above baseline ($p = 0.0110$) (Fig. 2C). At none of these three sites did ABP increase significantly during SSN activation. Thus, increased perfusion pressure due to increased ABP was unlikely to be a driver of the ChBF increases with SSN stimulation.

We additionally examined the effect of electrical activation of choroidal SSN with negative current pulses (mean of 17.3 μA) via a glass pipette at the nasal anterior recording site,

which also yielded significant ChBF increases, although the increases were lesser than with metal electrodes, presumably due to the lesser spread of current with the finer tipped glass micropipettes (Fig. 2D). The mean ChBF increases for rats with stimulation with glass pipettes were, nonetheless, significantly elevated above baseline by 20.5% ($p = 0.0097$), and the peak increases were significantly elevated above baseline by 30.9% ($p = 0.0094$). Mean systemic ABP during SSN stimulation, by contrast to the choroidal effects, was only 1.05% above basal, but nonetheless significant by a paired t -test ($p = 0.0090$) (Fig. 2D). As the overall analysis below of the correlations between ChBF on one hand, and ChBVol, ChBVel, and ABP on the other shows, however, increased choroidal perfusion pressure due to increased ABP was unlikely to be a driver of the large ChBF increases with choroidal SSN stimulation.

3.1.2. Choroidal SSN stimulation – relative contributions of volume and velocity to choroidal blood flow increases—

We also examined the effects of choroidal SSN stimulation at each of the three sites on ChBVol and ChBVel. For the rats assessed at the site temporal to the superior rectus (site 1 in Fig. 1), electrical activation of SSN yielded ChBF increases that were more velocity-driven (76.2% mean and 119.8% peak above baseline) than volume-driven (34.2% mean and peak 61.0% above baseline), with the mean and peak for the former significantly greater than baseline (mean: $p = 0.0391$; peak: $p = 0.0365$), but both only approaching significance for the latter (mean: $p = 0.1213$; peak: $p = 0.05859$) (Fig. 2A). We found similar effects of SSN stimulation at the anterior nasal site (site 2 in Fig. 1). The increase was again more velocity-driven (mean 99.4% above baseline) than volume-driven (mean 36.5% above baseline), with the mean and peak for velocity significantly greater than baseline (mean: $p = 0.0276$; peak: $p = 0.0391$), but not for volume (mean: $p = 0.2177$; peak: $p = 0.2279$) (Fig. 2B). At the posterior nasal site (site 3 in Fig. 1), the increase as well was more velocity-driven (mean 114.1% above baseline, and peak 180.8% above baseline) than volume-driven (mean 4.0% above baseline, and peak 20.7% above baseline), with ChBVel significantly greater than baseline for the mean increase ($p = 0.0476$) but not ChBVol ($p = 0.6206$) (Fig. 2C). Peak velocity at this site also trended toward significantly different than baseline ($p = 0.0600$). Across the three sites, however, there was a clear tendency for ChBVol to also be increased by choroidal SSN stimulation, albeit less so than ChBVel. Pooling the data across sites ($n = 12$), mean and peak ChBVol were seen to be significantly increased during stimulation (mean: $p = 0.0273$; peak: $p = 0.0063$).

In the case of electrical activation of choroidal SSN via a glass micropipette, (Fig. 2D), the mean and peak increases in ChBF at the nasal anterior site were more equally driven by volume and velocity increases. Significant 10.7% and 22.0% increases were seen for mean and peak choroidal blood volume ($p = 0.0126$ and $p = 0.0060$), respectively, and significant 9.8% and 15.1% increases were seen for mean and peak choroidal blood velocity ($p = 0.0310$ and $p = 0.0152$), respectively. The slightly different results with stimulation with glass micropipettes may reflect a relatively lesser recruitment of choroidal SSN neurons responsible for orbital vasodilation with the lesser current spread with glass than metal electrodes.

We used regression analysis to further assess the contributions of ABP, ChBVol and ChBVel to the observed ChBF increases with activation of choroidal SSN across all three sites and

both stimulating electrode types. We found that both ChBVol and ChBVel were significantly correlated with the ChBF increase, considering both the mean increase and the peak increase, but the correlation was higher and slope of the regression line greater for ChBVel than ChBVol (Fig. 3). For example, the correlation of mean ChBF during SSN stimulation with ChBVel was $r = 0.77653$ but the correlation with ChBVol was only $r = 0.52503$. Moreover, the slope of the mean ChBF regression line for ChBVel was 0.7321, but it was only 0.1892 for ChBVol. Similarly, the correlation of peak ChBF during SSN stimulation with ChBVel was $r = 0.8150$ but the correlation with ChBVol was only $r = 0.5596$, and the slope of the peak ChBF regression line for ChBVel was 0.7670, but it was only 0.1926 for ChBVol. By contrast, across these cases the mean and peak ABP changed little during choroidal SSN stimulation and showed no significant positive correlation with ChBF during SSN stimulation. Moreover, the slope of the relationship of ChBF with ABP was flat for both mean and peak ChBF (Fig. 3). Thus, ChBVel increases (presumably reflecting intra-orbital vessel vasodilation) were a greater contributor to ChBF increases during choroidal SSN stimulation than ChBVol increases (presumably reflecting intrachoroidal vasodilation), although both did contribute. Changes in ABP were, however, not significant contributors to the ChBF increase.

3.1.3. Choroidal SSN stimulation - choroidal blood flow dynamics—The relative ChBF, ChBVol, ChBVel and ABP changes prior to, during and after choroidal SSN stimulation were plotted for six of the rats with glass micropipette stimulation to further examine the hemodynamics of the effect of electrical stimulation of choroidal SSN on ChBF (Fig. 4). The ChBF increase reached its peak by about 5 s after current onset, declined slightly over the next 2 s of stimulation, and then rapidly declined and returned to baseline by about 6 s after stimulation offset. The increase in choroidal blood velocity (ChBVel) was coincident with the ChBF increase and peaked at about the same point after stimulation onset as the ChBF peak. ChBVol increased slightly more slowly initially than did ChBVel, and its peak was slightly later. Both ChBVol and ChBVel declined rapidly with stimulation offset, the latter more so. Choroidal SSN activation for these cases yielded a slight, gradual rise in ABP that did not begin until after about 3 s of stimulation, resulting in a peak ABP of 13.7% above baseline at 6.9 s after onset of SSN stimulation. The ABP quickly returned to basal levels by about 5 s after stimulation offset (Fig. 4).

3.1.4. Effect of NOS inhibition on ChBF increase during choroidal SSN stimulation—To evaluate the NO-dependence of SSN-mediated ChBF increases, we examined the effects of NPA on the evoked increases in four rats at the anterior nasal site (two with metal electrode stimulation and two with glass micropipette stimulation) and the effects of LNAME at the anterior temporal site in one rat (Fig. 5A). Across these rats, we found that NOS inhibition had no significant effect on mean basal ABP (6.0% above basal, $p = 0.1179$), consistent with nNOS rather than eNOS inhibition for the four NPA rats. NOS inhibition did slightly but significantly reduce mean basal ChBF (18.4% below basal $p = 0.0221$). The elevating effect of stimulation of choroidal SSN on mean and peak ChBF was also significantly diminished after NOS inhibition. For example, the mean ChBF increase with nNOS inhibition was 66.7% of that prior to NOS inhibition and no longer significantly different from baseline ($p = 0.0759$). Additionally, the mean ChBF during choroidal SSN

stimulation was significantly less after NOS inhibition than prior to inhibition ($p = 0.0033$). Similarly, the peak ChBF was only 63.1% of that prior to NOS inhibition, and the magnitude of the peak response was significantly less than prior to nNOS inhibition ($p = 0.0104$) (Fig. 5B). The effect of nNOS inhibition on the evoked ChBF increase appears to have been largely driven by an effect on ChBVel, since the blunting effects of nNOS inhibition on the mean and peak response trended or were significant for ChBVel (mean: $p = 0.0594$; peak: $p = 0.0418$), but were neither in the case of ChBVol (mean: $p = 0.3508$; peak: $p = 0.6336$).

3.2. Effects of choroidal SSN lesions

3.2.1. Effects of choroidal SSN lesion on scotopic ERG—We evaluated the effects of right choroidal SSN destruction on the scotopic ERG a-wave and b-waves over the 10-week period after the lesion in 11 rats, with rats tested at multiple time points over this period. To assess changes in rats with choroidal SSN lesion over time, we compared to pre-lesion values for 7 of these rats (not all were assessed pre-lesion) plus three more that received no lesion. To assess specificity of lesion effects, we also evaluated the scotopic ERG a-wave and b-waves over a 10-week period in 9 control rats in which the lesion did not include choroidal SSN, with rats again tested at multiple time points over this period. To assess changes over time for the SSN-miss rats, we compared to pre-lesion values for six of them (not all were assessed pre-lesion) plus the three more that received no lesion. The rats were sacrificed subsequent to ERG testing, and immunohistochemistry was carried out on the brain to assess choroidal SSN lesion accuracy, and thereby classify rats as SSN lesion cases (SSN-Lx) or SSN miss cases (SSN-miss). Immunolabeling for ChAT or nNOS, both of which are found in choroidal SSN neurons (Fig. 6), distinguished cases with choroidal SSN destruction from those in which the lesions missed choroidal SSN (Cuthbertson et al., 2003). The 11 cases classified as SSN-Lx averaged 83.7% loss of choroidal SSN, ranging from complete to 50% destruction. The 9 cases classified as SSN-miss included four cases that had electrode penetrations or lesions that were near choroidal SSN, yielding some slight loss of choroidal SSN neurons ranging from 5 to 10%. The penetrations in the remaining 5 miss cases were not near enough to SSN to yield any evident choroidal SSN neuron loss, and the overall mean loss for the SSN-miss cases was 2.8%. For both SSN-Lx and SSN-miss groups, we evaluated the change in scotopic ERG a-wave and b-wave peaks and latencies over time post lesion for both the left and right eyes, with assessments done pre-lesion, at about 4 weeks post lesion, and again at about 10 weeks post lesion.

For the eyes ipsilateral to right SSN-Lx, the scotopic ERG a-wave and b-wave peaks both showed a reduced amplitude compared to their pre-lesion control comparison group right eyes. In the case of the a-wave, the peak amplitudes with the brighter intensities were greater in control eyes than at either post-lesion time point in the SSN-Lx right eyes, with the deficit growing worse from 4 to 10 weeks (Fig. 7A). This was most evident at the $758 \text{ cd}\cdot\text{s}/\text{m}^2$ intensity, for which the a-wave peak in SSN-Lx right eyes was only 72.6% of control right eyes at about 4 weeks post lesion and 60.2% at about 10 weeks post lesion. Notably, the a-wave was already significantly reduced for the brightest 3 light intensities by about 4 weeks post lesion ($p = 0.0150$ by ANOVA), with the deficit slightly greater at about 10 weeks post lesion ($p = 0.0018$ by ANOVA). By contrast, the a-wave peak amplitudes in the right eyes of rats with lesions that missed choroidal SSN (Fig. 7B) did not differ significantly from their

control comparison group right eyes at the 4-week time point ($p = 0.4114$), although they did show a slight but significant reduction at the 10-week post lesion time point ($p = 0.0338$). Thus, the a-wave decrement in the eyes ipsilateral to choroidal SSN destruction at 4 weeks post lesion is largely a specific effect of the SSN destruction. The slight a-wave decrement at 10 weeks in the eyes ipsilateral to lesions that did not destroy choroidal SSN, however, either reflects some nonspecific lesion effect, or an effect on choroidal SSN due to its proximity to the lesion site in several of the choroidal SSN miss cases. In any case, the right eye a-wave deficit at 10 weeks relative to prelesion was greater in the rats with choroidal SSN destruction.

Right choroidal SSN destruction also impaired the b-wave in the eyes ipsilateral to the lesion, in this case with the abnormality being not significant until about 10 weeks post lesion ($p = 0.000006$), and overall amplitudes reduced by 23.6% at that time (Fig. 7C). In the case of the b-wave, the peak amplitudes in the right eyes of right SSN-miss rats did not differ significantly from prelesion control values at either the 4-week ($p = 0.4801$) or 10-week post lesion time points ($p = 1.0000$) (Fig. 7D). Thus, the b-wave decrement in the eyes ipsilateral to choroidal SSN destruction appears to be a specific effect of the choroidal SSN destruction. Note that the right eye b-wave to a-wave ratio for the two brightest light intensities did not differ significantly from control at 4 or 10 weeks in either SSN-Lx rats (4wk $p = 0.5121$; 10wk $p = 0.1368$), or SSN-miss rats (4wk $p = 0.6500$; 10wk $p = 0.2661$), suggesting comparable effects of SSN destruction on a-wave and b-wave.

Somewhat surprisingly, the right SSN destruction also had an impact on the a-wave and b-wave in the eye contralateral to the lesion, though less than for the right eye. In the case of the a-wave, the peak amplitudes for the brightest 3 light intensities for the left eye did not differ significantly from prelesion left eye values until 10 weeks post lesion ($p = 0.0016$) (Fig. 8A). The left eyes in rats with missed right choroidal SSN lesions, however, did not differ significantly from the prelesion control comparison group in their a-wave peak amplitudes at either the 4-week ($p = 0.3092$) or 10-week ($p = 0.0578$) time points (Fig. 8B). Similarly, the b-wave peak amplitude was also significantly reduced in the left eyes of rats at 10 weeks after right choroidal SSN destruction, by about 27.4% compared to prelesion control left eye values ($p = 0.000026$) (Fig. 8C), and again no such b-wave amplitude reduction was seen for the left eyes in rats with missed right choroidal SSN lesions at either 4 weeks ($p = 0.7147$) or 10 weeks ($p = 0.5221$) post lesion (Fig. 8D). The left eye b-wave to a-wave ratio for the two brightest light intensities also did not differ significantly from control at 4 or 10 weeks in either SSN-Lx rats (4wk $p = 0.8410$; 10wk $p = 0.6491$) or SSN-miss rats (4wk $p = 0.4936$; 10wk $p = 1.000$). The reasons why the right choroidal SSN destruction might have had an impact on the left eye a-wave and b-wave are considered in the Discussion.

3.2.2. Effect of choroidal SSN lesion on choroidal baroregulation—The impact of variation in ABP on ChBF was assessed for right eyes of three rats with choroidal SSN-Lx and right eyes of three rats in which the lesion missed SSN. To assess choroidal baroregulation, we plotted ChBF as a function of ABP, with both normalized to baseline for each animal, divided into progressive ABP bins of 5 mmHg, and calculated group means for each bin (Fig. 9), as in our prior studies of baroregulation (Li et al., 2018; Reiner et al, 2010,

2011). The slope of the relationship between ABP and ChBF over the low ABP range (i.e. <100% of basal ABP) approached 1 for the eyes ipsilateral to choroidal SSN destruction (slope = 0.6132), and ABP and ChBF were highly correlated ($r = 0.716$). Thus, choroidal SSN destruction impaired the ability of ChBF to compensate and thereby remain stable as ABP decreased, due apparently to a loss of centrally mediated parasympathetic vasodilation of the choroid (Fig. 9A). Nonetheless, for the eyes ipsilateral to choroidal SSN destruction, ChBF remained relatively flat at ABP greater than 100% of basal. By contrast, baroregulation during both low ABP and high ABP was normal in eyes ipsilateral to lesions that missed SSN, (Fig. 9B), with the slope of the ABP-ChBF relationship and the ABP-ChBF correlation approaching zero in both cases.

3.2.3. Geographic extent of parasympathetic and sympathetic choroidal innervation and effect of choroidal SSN lesion—We examined choroidal innervation by parasympathetic and sympathetic fibers in normal rats and rats with choroidal SSN destruction, to evaluate the topographic distribution of the choroidal innervation and assess if it was altered by choroidal SSN destruction. Immunostaining of parasympathetic choroidal fibers for nNOS or VIP showed the parasympathetic innervation to be present throughout the geographic extent of the eye (Fig. 10A–D), and be not obviously altered by choroidal SSN destruction (Fig. 10E and F). Similarly, immunostaining of sympathetic choroidal fibers for VMAT2 (vesicular monoamine transporter 2) showed that they too were present throughout the geographic extent of the eye, and not obviously altered by choroidal SSN destruction (Fig. 10G and H).

3.2.4. Effect of choroidal SSN lesion on the abundance of GFAP+ müller cell processes—We sought to determine if impairment of adaptive control of ChBF by the choroidal SSN-PPG circuit was associated with retinal pathology, as reflected by increased GFAP immunolabeling of retinal Müller cell processes. Rats ($n = 19$) were sacrificed nine to twenty weeks after attempted destruction of choroidal SSN (mean = 12.8 weeks), in some cases after prior ERG assessment. Histological analysis of hindbrain sections for these rats revealed that twelve had successful destruction of choroidal SSN and seven did not. Immunolabeling revealed that in the rats with SSN-Lx, GFAP immunolabeling was increased in retinal Müller cell processes throughout the ipsilateral retina (Fig. 11), and in contralateral retina as well. The GFAP immunolabeled Müller cell processes in the eyes from SSN-Lx rats in many cases traversed the inner plexiform layer (IPL). By contrast, in control cases, which included four normal rats with no lesion attempt and the seven cases with lesions that missed choroidal SSN, GFAP immunolabeling was mainly limited to the nerve fiber layer and ganglion cell layer, and rarely extended much beyond the ganglion cell layer (Fig. 11). Using a scoring system that reflects both the abundance of GFAP immunolabeled processes and the extent of their penetration into the retina (Kimble et al., 2006), we found that the GFAP immunolabeled Müller cell processes in SSN-Lx retinas were significantly increased ($p < 0.0135$) for both eyes compared to control (Fig. 12). The reasons why the right SSN destruction might have had an impact on left eye GFAP+ Müller cell processes, as it had for left eye ERG, are considered in the Discussion.

3.2.5. Effect of choroidal SSN lesion on retinal GFAP expression—We also assessed GFAP expression after SSN-Lx by qPCR, comparing right and left retina in two rats that survived a mean of 11 days after SSN-Lx compared to right and left retina from 3 control rats with no lesion and two rats with lesions that largely spared choroidal SSN. We found that GFAP was significantly increased 8-fold by SSN-Lx ($p = 0.0110$).

4. Discussion

Our studies indicate that the parasympathetic innervation of choroid by the SSN-PPG circuit mediates a choroid-wide increase in ChBF. In conjunction with our prior work on central SSN circuitry connectivity and function (Li et al, 2010, 2015, 2016a, 2016b; Reiner et al., 2010) and the present work on the adverse effects of choroidal SSN destruction on ChBF baroregulation, our studies indicate that the parasympathetic regulation of choroid mediates a vasodilatory compensation during downward fluctuations in ABP that serves to maintain stable ChBF. Impairment of this autonomic control would, thus, be expected to cause significant episodic insufficiency of ChBF, compounded by the effects of reduced basal flow. Consistent with the chronic hypoxic and ischemic stress such choroidal underperfusion would be expected to cause (Feigl, 2009), we found that disruption of parasympathetic regulation of ChBF harms retina, as we found it to be associated with reductions in the scotopic ERG a-wave and b-wave peaks and Müller glial cell activation within months of the perturbation. These findings and their implications for age-related decline in parasympathetic control of ChBF, and other diseases and conditions exhibiting reduced ChBF, are discussed in more detail below.

4.1. Parasympathetic control of choroidal blood flow

The PPG profusely innervates choroidal and orbital blood vessels with fibers co-containing VIP and nNOS, with the postganglionic axons from the PPG entering the choroid directly on the choroidal feeder vessels and by joining the short ciliary nerves from the ciliary ganglion to the choroid (Reiner et al, 2012, 2018). Numerous studies indicate that VIP and NO derived from PPG terminals on orbital and choroidal blood vessels exert a vasodilatory influence on them (summarized in Reiner et al., 2018, 2012). The PPG in mammals receives its preganglionic parasympathetic input from SSN (Cuthbertson et al., 2003; Li et al., 2015; Ten Tusscher et al., 1990), with those preganglionic neurons controlling choroid slightly more rostral and medial than those controlling other PPG targets, such as the Meibomian glands (LeDoux et al., 2001) and the lacrimal gland (Tóth et al., 1999). Activation of preganglionic input to the PPG by facial nerve stimulation yields a ChBF increase, that appears to be mediated by both NO and VIP released from PPG terminals (Nilsson, 1996, 2000; Nilsson et al, 1984, 1985; Stjernschantz and Bill, 1980). As the studies addressing these points used radiolabeled microspheres to measure ChBF, they could not provide information on the regional nature of ChBF control by the SSN input to the PPG.

Using transcleral laser Doppler flowmetry (LDF) to measure ChBF at anterior sites along the upper surface of the rat eye, Steinle et al. (2000) reported large increases with direct SSN stimulation, which could be significantly decreased by prior intravenous administration of the general NOS inhibitor LNAME or the nNOS-selective inhibitor TRIM (1-(2-

Trifluoromethylphenyl)imidazole). Steinle et al. (2000), however, did not detect ChBF increases in posterior choroid with SSN stimulation, raising the possibility that PPG control of ChBF was limited in its regional extent. Our present work shows that SSN activation of PPG input to the orbit drives a ChBF increase at anterior and posterior choroidal sites. In light of this and in light of our evidence for PPG innervation of choroid throughout the regional extent of the eye, it is highly likely that the SSN-PPG circuit drives ChBF increases in all geographic sectors of the eye, and at least in part mediated by the vasodilatory action of NO. It may be that Steinle et al. (2000) did not detect ChBF increases in posterior choroid of rats with SSN stimulation because their approach of slitting the cornea to access the posterior retina eliminated intraocular pressure (IOP) and thereby compromised choroidal vasodilation in response to preganglionic activation. Note that studies in cats and rabbits have shown parasympathetic regulation of ChBF in the posterior pole of the eye in preparations in which IOP was maintained (Kiel, 1999; Mann et al., 1995; Riva et al., 1994).

In prior studies, we demonstrated excitatory input to choroidal SSN from several central brain areas that play a role in maintaining stable systemic ABP (Li et al, 2010, 2015), including the caudolateral part of the NTS, as well as the dorsal part of the paraventricular nucleus (PVN) of the hypothalamus, the raphe magnus (RaM), the B3 serotonergic cell group of the pons, the A5 noradrenergic group of the pons, and the rostral ventrolateral medulla (RVLM). Since the projection from NTS to choroidal SSN, in particular, appeared to provide a means by which ABP signals can modulate ChBF, in a prior study we confirmed that activation of baroreceptive NTS evoked ChBF increases in rat eye (recording from what is here called the anterior nasal site), driven by increases in both ChBVol presumably caused by choroidal vasodilation, and ChBVel presumably caused by orbital vessel dilation (Li et al., 2016b). The increases in ChBF with NTS stimulation were significantly reduced by intravenous administration of NPA, thus implicating intrachoroidal and orbital nitrenergic PPG terminals in the NTS-elicited ChBF increases. Our present findings with choroidal SSN stimulation also indicate that ChBF is increased by both vasodilation of orbital and choroidal vessels, and partly mediated by NO. Our overall studies, thus, suggest a role of the input of baroresponsive NTS to choroidal SSN in the blood pressure-dependent regulation of ChBF. Our present studies showing that, like with nNOS inhibition (Reiner et al., 2010), choroidal SSN destruction impairs choroidal baroregulation during low systemic ABP directly supports this conclusion.

4.2. Parasympathetic control of choroidal blood flow and retinal health

Reflexive PPG-mediated choroidal vasodilation could be important for maintaining stable ChBF and thereby metabolic support of the retina during the routine, daily bouts of low ABP, such as might occur during inactivity, rest, or sleep, as well as for preventing retinal hypoxia and ischemia during extreme ABP-lowering events due to injury or blood loss (Bill, 1985; Bill and Sperber, 1990). In the present study, we found that electrolytic destruction of the right choroidal part of SSN significantly diminished the right eye ERG a-wave and b-wave amplitudes by 10 weeks after ipsilateral SSN destruction, with the deficit already evident for the a-wave by about 4 weeks post lesion. By contrast, animals with no lesion or lesions that missed right choroidal SSN (SSN-miss) showed no b-wave deficit, and only a lesser a-wave deficit (perhaps attributable to the proximity of some of the SSN misses to

choroidal SSN). Surprisingly, left eye a-wave and b-wave abnormalities were also seen in the SSN-Lx rats (but not SSN miss rats). In the immunohistochemical evaluation of the impact of the right SSN lesion on the retina, we found that retinal GFAP expression and GFAP immunolabeling of Müller cell processes traversing the IPL were significantly upregulated throughout the ipsilateral retina in SSN-Lx rats. Again, we observed that the left eye was also affected, with GFAP+ Müller cell processes significantly increased in the left retina as well. The contralateral effect of choroidal SSN destruction is somewhat surprising, since the SSN projection to the PPG is thought to be exclusively ipsilateral (Cuthbertson et al., 2003; Li et al, 2010, 2015; Tóth et al., 1999). In the course of the present studies involving evaluation of the accuracy of the stimulation sites in right choroidal SSN by cfos immunolabeling, we did, however, note that such stimulation invariably yielded a few cfos+ neurons in the left choroidal SSN. This suggestion of a projection from one choroidal SSN to the other was supported when we re-examined pathway tracing cases from our prior studies on choroidal SSN inputs (Li et al, 2010, 2015). In particular, in cases with BDA3k retrograde tracer injection into right SSN, we observed a few BDA3k+ perikarya in left choroidal SSN. Thus, lesions of right choroidal SSN may have damaged this contralateral projection and thereby impaired the functioning of the choroidal SSN-PPG circuit of the left eye. It is also possible that the astrocyte network linking the two eyes via the optic nerves and chiasm leads to a redistribution of metabolic resources between the eyes that leads both eyes to be affected by unilateral choroidal SSN destruction (Cooper et al., 2020). The more delayed nature of the a-wave ERG abnormalities for the left eye after right SSN destruction is consistent with a lesser or more protracted injury process, mediated indirectly by astrocytes for example, than for the right eye. Note that we also observed a contralateral effect of impairing parasympathetic control of choroidal blood flow in our studies of the effects of lesions of the medial part of the nucleus of Edinger-Westphal in pigeons (Kimble et al., 2006).

Our present results are reminiscent of our findings in mice lacking a nNOS allele (Reiner et al., 2018), which would be expected to result in diminished NO-mediated control of ChBF by the parasympathetic nervous system. Using transcleral laser Doppler flowmetry as in the present study, we found that basal ChBF was ~60% of WT in nNOS ± mice at 3 months of age, likely due to reduced NO production to maintain basal ChBF, but baroregulation at this age appeared to be largely intact (perhaps due to compensation by VIP or cholinergic mechanisms) (Dick et al., 2002; Meng et al., 1996). Visual acuity did not differ between wild-type (WT) and mutant mice at 3 months of age, but was only 60% of age-matched WT in nNOS ± mice at 200–500 days of age. Moreover, a significant decline in photoreceptor abundance was seen between 200 and 500 days of age in nNOS ± mice. These findings in mice, as well as those presented here for rats, indicate that parasympathetic choroidal vasodilation appears important for long-term outer retinal health, and NO-mediated vasodilation is an important contributor to this. The loss of the parasympathetic control appears to cause both chronic reduced basal flow at basal ABP and yet more profound vascular insufficiency during systemic hypotensive episodes (Reiner et al., 2010). It is likely the diminished oxygen tension resulting from the choroidal underperfusion causes ischemic stress and vascular insufficiency in outer retina that sets in motion oxidative and

inflammatory processes that in the long-term compromise retinal health and function (Feigl, 2009; Osborne et al., 2004).

4.3. Implications of current findings

As reviewed in our prior papers (Reiner et al, 2012, 2018), many diseases affecting the retina have impaired ChBF and/or diminished choroidal innervation as concomitants, including age-related macular degeneration (AMD), chronic hypertension, insulin-dependent diabetes, glaucoma, ischemic outer retinal disease, and central serous chorioretinopathy. Additionally, impaired ChBF regulation and diminished sympathetic and parasympathetic choroidal innervation is observed in aging (Reiner et al., 2012, 2018). Thus, the available data are consistent with the view that disturbances in maintenance of basal neurogenic choroidal tone and/or adaptive neural control of ChBF could be contributing factors to the retinal declines seen in humans and other species in hypertension, diabetes, glaucoma, ischemic retinal disease, and central serous chorioretinopathy, and with aging. Clearly other mechanisms also contribute to retinal damage in these conditions, such as edema, retinal detachment and/or neovascularization (Frank, 1988; Tso and Jampol, 1990; Tso, 1988). It is also possible that in some cases the altered ChBF control is secondary to the disease. Moreover, loss and narrowing of submacular choroidal vessels, as seen in normal aged eyes, may also contribute to ChBF abnormalities (Grunwald et al., 1998a; Ramrattan et al., 1994; Spraul et al., 1996). Nonetheless, the possibility that impaired neurogenic regulation of ChBF directly promotes degeneration in these diseases and in aging needs to be considered.

Much of the attention on disease-related ChBF impairments has focused on reductions in ChBF, as would occur with impaired parasympathetic control. Nonetheless, sympathetic control of choroid is also impaired with aging (Nuzzi et al., 1996; Smith et al., 2007), and defects in choroidal baroregulation during high systemic blood pressure occur in aging (Dallinger et al., 1998; Reiner et al., 2011), and in wet AMD (Pournaras et al., 2006). Recent studies by the Schmetterer group (Told et al., 2013) have shown that at least some genetic risk factors for AMD, such as the Y402H complement factor H (CFH) polymorphism, may themselves compromise autonomic sympathetic ChBF control early in life. The observation that CFH-deficient mice show progressive choroidal pathology further underscores a possible direct effect of pro-AMD polymorphisms on neurogenic control of ChBF (Von Leithner et al., 2009). Consistent with the premise that impaired autonomic regulation of ChBF early in life could contribute to AMD pathogenesis, we and others have shown an adverse effect of sympathetic denervation of the rat choroid on the health and functioning of the retina (Dieguez et al., 2018, 2019, 2020; Li et al., 2018). As we have shown here, impaired parasympathetic control of ChBF is also harmful to the health of the retina, with abnormalities evident within months of the ChBF disruption. Underscoring the possible contribution of defects in parasympathetic hypotensive baroregulation to AMD, Bhutto et al. (2010) have reported deficiency in choroidal nNOS innervation in AMD patients. Thus, chronic impairment of both sympathetic and/or parasympathetic regulation of ChBF beginning in early adulthood, driven by genetic AMD risk factors, may contribute to AMD progression.

5. Conclusions

Our study using electrical stimulation of choroidal SSN indicates that activation of preganglionic parasympathetic input increases ChBF at diverse sites along the superior aspect of the eye. Our immunohistochemical evidence showing parasympathetic fibers distributed throughout the regional extent of the choroid indicates that choroidal SSN is likely to drive vasodilation throughout the regional extent of the choroid. The parasympathetic influence on ChBF is partially mediated by nitrenergic postganglionic terminals. Our study of the effects of lesions of choroidal SSN indicates that choroidal baroregulation is impaired by disruption of the parasympathetic input to the choroid. Such disturbance in the adaptive parasympathetic regulation of ChBF leads to functional disruption and morphological damage in the retina.

Acknowledgements

Special thanks to Aminah Henderson, Marion Joni, Ting Wong, Julia Jones, and Dr. Seth Jones for assistance and/or advice during the course of our studies. Our work has been supported by the National Institutes of Health (grant number EY-005298) (AR), The Methodist Hospitals Endowed Professorship in Neuroscience (AR), the University of Tennessee Neuroscience Institute (CL), and the Department of Ophthalmology of the University of Tennessee Health Science Center (MECF), the National Science Foundation (grant number DUE 9850780) (MECF), the Assisi Foundation (MECF), and an unrestricted grant from Research to Prevent Blindness (MECF).

References

- Alm A, 1992. Ocular circulation. In: Hart WM (Ed.), *Adler's Physiology of the Eye: Clinical Application*. Mosby, St Louis, pp. 198–227.
- Alm A, Bill A, 1973. The effect of stimulation of the cervical sympathetic chain on retinal oxygen tension and on uveal, retinal and cerebral blood flow in cats. *Acta Physiol. Scand* 88, 84–94. 10.1111/j.1748-1716.1973.tb05436.x. [PubMed: 4751166]
- Bhutto IA, Baba T, Merges C, McLeod DS, Luttly GA, 2010. Low nitric oxide synthases (NOSs) in eyes with age-related macular degeneration (AMD). *Exp. Eye Res* 90, 155–167. [PubMed: 19836390]
- Bill A, 1985. Some aspects of the ocular circulation. *Invest. Ophthalmol. Vis. Sci* 26, 410–424. [PubMed: 3980165]
- Bill A, Sperber GO, 1990. Control of retinal and choroidal blood flow. *Eye* 4 (Pt2), 319–325. 10.1038/eye.1990.43. [PubMed: 2199239]
- Braun RD, Linsenmeier RA, 1995. Retinal oxygen tension and the electroretinogram during arterial occlusion in the cat. *Investig. Ophthalmol. Vis. Sci* 36, 523–541. 10.1097/00006982-199616020-00031. [PubMed: 7890484]
- Collier RH, 1967. Experimental embolic ischemia of the choroid. *Arch. Ophthalmol* 77, 683–692. 10.1001/archoph.1967.00980020685025. [PubMed: 6022740]
- Cooper GR, Mialkowski K, Wolff DJ, 2000. Cellular and enzymatic studies of N (ω)-propyl-L-arginine and S-ethyl-N- [4-(trifluoromethyl)phenyl]isothiourea as reversible, slowly dissociating inhibitors selective for the neuronal nitric oxide synthase isoform. *Arch. Biochem. Biophys* 375, 183–194. 10.1006/abbi.1999.1658. [PubMed: 10683266]
- Cooper ML, Pasini S, Lambert WS, D'Alessandro KB, Yao V, Risner ML, Calkins DJ, 2020. Redistribution of metabolic resources through astrocyte networks mitigates neurodegenerative stress. *Proc. Natl. Acad. Sci. U.S.A* 117 (31), 18810–18821. 10.1073/pnas.2009425117. [PubMed: 32690710]
- Cuthbertson S, LeDoux MS, Jones S, Jones J, Zhou Q, Gong S, Ryan P, Reiner A, 2003. Localization of preganglionic neurons that innervate choroidal neurons of pterygopalatine ganglion. *Invest. Ophthalmol. Vis. Sci* 44, 3713–3724. 10.1167/iovs.02-1207. [PubMed: 12939284]

- Dallinger S, Findl O, Strenn K, Eichler HG, Wolzt M, Schmetterer L, 1998. Age dependence of choroidal blood flow. *J. Am. Geriatr. Soc* 46, 484–487. 10.1111/j.1532-5415.1998.tb02471.x. [PubMed: 9560073]
- Deng YP, Xie JP, Wang HB, Lei WL, Chen Q, Reiner A, 2007. Differential localization of the GluR1 and GluR2 subunits of the AMPA-type glutamate receptor among striatal neuron types in rats. *J. Chem. Neuroanat* 33, 167–192. 10.1016/j.jchemneu.2007.02.008. [PubMed: 17446041]
- Dick JMC, Van Molle W, Brouckaert P, Lefebvre RA, 2002. Relaxation by vasoactive intestinal polypeptide in the gastric fundus of nitric oxide synthase-deficient mice. *J. Physiol* 538, 133–143. 10.1113/jphysiol.2001.012906. [PubMed: 11773322]
- Diéguez HH, González Fleitas MF, Aranda ML, Calanni JS, Keller Sarmiento MI, Chianelli MS, Alaimo A, Sande PH, Romeo HE, Rosenstein RE, Dorfman D, 2020. Melatonin protects the retina from experimental nonexudative age-related macular degeneration in mice. *J. Pineal Res* 68 (4), e12643 10.1111/jpi.12643. [PubMed: 32133696]
- Dieguez HH, Romeo HE, Alaimo A, González Fleitas MF, Aranda ML, Rosenstein RE, Dorfman D, 2019. Oxidative stress damage circumscribed to the central temporal retinal pigment epithelium in early experimental non-exudative age-related macular degeneration. *Free Radic. Biol. Med* 131, 72–80. 10.1016/j.freeradbiomed.2018.11.035. [PubMed: 30502459]
- Dieguez HH, Romeo HE, González Fleitas MF, Aranda ML, Milne GA, Rosenstein RE, Dorfman D, 2018. Superior cervical gangliectomy induces nonexudative age-related macular degeneration in mice. *DMM Dis. Model. Mech* 11, dmm031641 10.1242/dmm.031641.
- Feigl B, 2009. Age-related maculopathy - linking aetiology and pathophysiological changes to the ischaemia hypothesis. *Prog. Retin. Eye Res* 28, 63–86. [PubMed: 19070679]
- Fitzgerald MEC, Gamlin PDR, Zagvazdin YS, Reiner A, 1996. Central neural circuits for the light-mediated reflexive control of choroidal blood flow in the pigeon eye: a laser Doppler study. *Vis. Neurosci* 13, 655–699. 10.1017/S095252380008555. [PubMed: 8870223]
- Fitzgerald MEC, Tolley E, Frase S, Zagvazdin YS, Miller RF, Hodos W, Reiner A, 2001. Functional and morphological assessment of age-related changes in the choroid and outer retina in pigeons. *Vis. Neurosci* 18, 299–317. 10.1017/S0952523801182143. [PubMed: 11417804]
- Fitzgerald MEC, Tolley E, Jackson B, Zagvazdin YS, Cuthbertson SL, Hodos W, Reiner A, 2005. Anatomical and functional evidence for progressive age-related decline in parasympathetic control of choroidal blood flow in pigeons. *Exp. Eye Res* 81, 478–491. 10.1016/j.exer.2005.03.008. [PubMed: 15935343]
- Fitzgerald MEC, Vana BA, Reiner A, 1990. Control of choroidal blood flow by the nucleus of Edinger-Westphal in pigeons: a laser Doppler study. *Investig. Ophthalmol. Vis. Sci* 31, 2483–2492. [PubMed: 2265988]
- Frank RN, 1988. Studies in diabetic retinopathy. In: Tso M (Ed.), *Retinal Disease: Biomedical Foundations & Clinical Management*. Lippincott Co., Philadelphia, pp. 165–180.
- Grunwald JE, Hariprasad SM, Dupont J, 1998a. Effect of aging on foveolar choroidal circulation. *Arch. Ophthalmol* 116, 150–154. 10.1001/archoph.116.2.150. [PubMed: 9488265]
- Grunwald JE, Hariprasad SM, DuPont J, Maguire MG, Fine SL, Brucker AJ, Maguire AM, Ho AC, 1998b. Foveolar choroidal blood flow in age-related macular degeneration. *Invest. Ophthalmol. Vis. Sci* 39, 385–390. [PubMed: 9477998]
- Grunwald JE, Metelitsina TI, DuPont JC, Ying GS, Maguire MG, 2005. Reduced foveolar choroidal blood flow in eyes with increasing AMD severity. *Invest. Ophthalmol. Vis. Sci* 46, 1033–1038. 10.1167/iovs.04-1050. [PubMed: 15728562]
- Hayreh SS, 2004. Posterior ciliary artery circulation in health and disease: the Weisenfeld lecture. *Invest. Ophthalmol. Vis. Sci* 45, 749–757. 10.1167/iovs.03-0469. [PubMed: 14985286]
- Honig MG, Del Mar N, Henderson DL, Ragsdale TD, Doty JB, Driver JH, Li C, Fortugno AP, Mitchell WM, Perry AM, Moore BM, Reiner A, 2019. Amelioration of visual deficits and visual system pathology after mild TBI via the cannabinoid type-2 receptor inverse agonism of raloxifene. *Exp. Neurol* 322, 13063 10.1016/j.expneurol.2019.113063.
- Ito YN, Mori K, Young-Duvall J, Yoneya S, 2001. Aging changes of the choroidal dye filling pattern in indocyanine green angiography of normal subjects. *Retina* 21, 237–242. 10.1097/00006982-200106000-00007. [PubMed: 11421013]

- Kiel JW, 1999. Modulation of choroidal autoregulation in the rabbit. *Exp. Eye Res* 69, 413–429. 10.1006/exer.1999.0717. [PubMed: 10504275]
- Kiel JW, Shepherd AP, 1992. Autoregulation of choroidal blood flow in the rabbit. *Invest. Ophthalmol. Vis. Sci* 33, 2399–2410. [PubMed: 1634337]
- Kimble TDH, Fitzgerald MEC, Reiner A, 2006. Sustained upregulation of glial fibrillary acidic protein in Müller cells in pigeon retina following disruption of the parasympathetic control of choroidal blood flow. *Exp. Eye Res* 83, 1017–1030. 10.1016/j.exer.2006.05.006. [PubMed: 16839546]
- LeDoux MS, Zhou Q, Murphy RB, Greene ML, Ryan P, 2001. Parasympathetic innervation of the meibomian glands in rats. *Invest. Ophthalmol. Vis. Sci* 42, 2434–2441. [PubMed: 11581180]
- Li C, Fitzgerald MEC, Del Mar N, Cuthbertson-Coates S, LeDoux MS, Gong S, Ryan JP, Reiner A, 2015. The identification and neurochemical characterization of central neurons that target parasympathetic preganglionic neurons involved in the regulation of choroidal blood flow in the rat eye using pseudorabies virus, immunolabeling and conventional pathway. *Front. Neuroanat* 9 10.3389/fnana.2015.00065. Article 65.
- Li C, Fitzgerald MEC, Del Mar N, Haughey C, Reiner A, 2018. Defective choroidal blood flow baroregulation and retinal dysfunction and pathology following sympathetic denervation of choroid. *Investig. Ophthalmol. Vis. Sci* 59 (12), 5032–5044. 10.1167/iops.18-24954. [PubMed: 30326072]
- Li C, Fitzgerald MEC, Del Mar N, Reiner A, 2016a. Disinhibition of neurons of the nucleus of solitary tract that project to the superior salivatory nucleus causes choroidal vasodilation: implications for mechanisms underlying choroidal baroregulation. *Neurosci. Lett* 633, 106–111. 10.1016/j.neulet.2016.09.029. [PubMed: 27663135]
- Li C, Fitzgerald MEC, Ledoux MS, Gong S, Ryan P, Del Mar N, Reiner A, 2010. Projections from the hypothalamic paraventricular nucleus and the nucleus of the solitary tract to prechoroidal neurons in the superior salivatory nucleus: pathways controlling rodent choroidal blood flow. *Brain Res.* 1358, 123–139. 10.1016/j.brainres.2010.08.065. [PubMed: 20801105]
- Li C, Fitzgerald MEC, Del Mar N., Reiner A, 2016b. Stimulation of baroresponsive parts of the nucleus of the solitary tract produces nitric oxide-mediated choroidal vasodilation in rat eye. *Front. Neuroanat* 10 10.3389/fnana.2016.00094. Article 94.
- Linsenmeier RA, Mines AH, Steinberg RH, 1983. Effects of hypoxia and hypercapnia on the light peak and electroretinogram of the cat. *Investig. Ophthalmol. Vis. Sci* 24, 37–46. [PubMed: 6826313]
- Linsenmeier RA, Steinberg RH, 1986. Mechanisms of hypoxic effects on the cat DC electroretinogram. *Invest. Ophthalmol. Vis. Sci* 27, 1385–1394. [PubMed: 3744728]
- Loeffler KU, Hayreh SS, Tso MOM, 1994. The effects of simultaneous occlusion of the posterior ciliary artery and vortex veins: a histopathologic study. *Arch. Ophthalmol* 112, 674–682. 10.1001/archophth.1994.01090170118033. [PubMed: 8185526]
- Lovaski JV, Kergoat H, Riva CE, Petrig BL, Geiser M, 2003. Choroidal blood flow during exercise-induced changes in the ocular perfusion pressure. *Invest. Ophthalmol. Vis. Sci* 44, 2126–2132. 10.1167/iops.02-0825. [PubMed: 12714652]
- Mann RM, Riva CE, Stone RA, Barnes GE, Cranston SD, 1995. Nitric oxide and choroidal blood flow regulation. *Investig. Ophthalmol. Vis. Sci* 36, 925–930. [PubMed: 7706041]
- Meng W, Ma J, Ayata C, Hara H, Huang PL, Fishman MC, Moskowitz MA, 1996. ACh dilates pial arterioles in endothelial and neuronal NOS knockout mice by NO-dependent mechanisms. *Am. J. Physiol.* 271- Hear. *Circ. Physiol* 40, H1145–H1150. 10.1152/ajpheart.1996.271.3.h1145.
- Metelitsina TI, Grunwald JE, DuPont JC, Ying GS, Brucker AJ, Dunaief JL, 2008. Foveolar choroidal circulation and choroidal neovascularization in age-related macular degeneration. *Invest. Ophthalmol. Vis. Sci* 49, 358–363. 10.1167/iops.07-0526. [PubMed: 18172113]
- Nilsson SFE, 2000. The significance of nitric oxide for parasympathetic vasodilation in the eye and other orbital tissues in the cat. *Exp. Eye Res* 70, 61–72. 10.1006/exer.1999.0752. [PubMed: 10644421]
- Nilsson SFE, 1996. Nitric oxide as a mediator of parasympathetic vasodilation in ocular and extraocular tissues in the rabbit. *Invest. Ophthalmol. Vis. Sci* 37, 2110–2119. [PubMed: 8814150]

- Nilsson SFE, Bill A, 1984. Vasoactive intestinal polypeptide (VIP): effects in the eye and on regional blood flows. *Acta Physiol. Scand* 121, 385–392. 10.1111/j.1748-1716.1984.tb07470.x. [PubMed: 6148840]
- Nilsson SFE, Linder J, Bill A, 1985. Characteristics of uveal vasodilation produced by facial nerve stimulation in monkeys, cats and rabbits. *Exp. Eye Res* 40, 841–852. 10.1016/0014-4835(85)90129-0. [PubMed: 2862056]
- Nuzzi R, Finazzo C, Grignolo FM, 1996. Changes in adrenergic innervation of the choroid during aging. *J. Fr. Ophthalmol* 19, 89–96. [PubMed: 8731776]
- Osborne NN, Casson RJ, Wood JPM, Chidlow G, Graham M, Melena J, 2004. Retinal ischemia: mechanisms of damage and potential therapeutic strategies. *Prog. Retin. Eye Res* 23, 91–147. 10.1016/j.preteyeres.2003.12.001. [PubMed: 14766318]
- Paxinos G, Watson C, 2009. *The Rat Brain in Stereotaxic Coordinates*, sixth. Academic Press, New York.
- Pournaras CJ, Logean E, Riva CE, Petrig BL, Chamot SR, Coscas G, Soubrane G, 2006. Regulation of subfoveal choroidal blood flow in age-related macular degeneration. *Invest. Ophthalmol. Vis. Sci* 47, 1581–1586. 10.1167/iovs.05-0434. [PubMed: 16565395]
- Ramrattan RS, Van der Schaft TL, Mooy CM, De Bruijn WC, Mulder PGH, De Jong PTVM, 1994. Morphometric analysis of Bruch's membrane, the choriocapillaris, and the choroid in aging. *Invest. Ophthalmol. Vis. Sci* 35, 2857–2864. [PubMed: 8188481]
- Reiner A, Del Mar N, Zagvazdin YS, Li C, Fitzgerald MEC, 2011. Age-related impairment in choroidal blood flow compensation for arterial blood pressure fluctuation in pigeons. *Invest. Ophthalmol. Vis. Sci* 52, 7238–7247. 10.1167/iovs.10-6464. [PubMed: 21828151]
- Reiner A, Fitzgerald MEC, Del Mar N, Li C, 2018. Neural control of choroidal blood flow. *Prog. Retin. Eye Res* 64, 96–130. 10.1016/j.preteyeres.2017.12.001. [PubMed: 29229444]
- Reiner A, Fitzgerald MEC, Li C, 2012. Neural control of ocular blood flow. In: Schmetter L, Kiel J (Eds.), *Ocular Blood Flow*. Springer-Verlag, Heidelberg, Germany, pp. 243–309. 10.1007/978-3-540-69469-4_12.
- Reiner A, Li C, Del Mar N, Fitzgerald MEC, 2010. Choroidal blood flow compensation in rats for arterial blood pressure decreases is neuronal nitric oxide-dependent but compensation for arterial blood pressure increases is not. *Exp. Eye Res* 90, 734–741. 10.1016/j.exer.2010.03.006. [PubMed: 20302861]
- Reiner A, Zagvazdin YS, Fitzgerald MEC, 2003. Choroidal blood flow in pigeons compensates for decreases in arterial blood pressure. *Exp. Eye Res* 76, 273–282. 10.1016/S0014-4835(02)00316-0. [PubMed: 12573656]
- Riva CE, Cranstoun SD, Mann RM, Barnes GE, 1994. Local choroidal blood flow in the cat by laser Doppler flowmetry. *Invest. Ophthalmol. Vis. Sci* 35, 608–618. [PubMed: 8113011]
- Smith CP, Sharma S, Steinle JJ, 2007. Age-related changes in sympathetic neurotransmission in rat retina and choroid. *Exp. Eye Res* 84, 71–81. 10.1016/j.exer.2006.08.018.
- Spraul CW, Lang GE, Grossniklaus HE, 1996. Morphometric analysis of the choroid, Bruch's membrane, and retinal pigment epithelium in eyes with age-related macular degeneration. *Invest. Ophthalmol. Vis. Sci* 37, 2724–2735. [PubMed: 8977488]
- Steinle JJ, Krizsan-Agbas D, Smith PG, 2000. Regional regulation of choroidal blood flow by autonomic innervation in the rat. *Am. J. Physiol. Regul. Integr. Comp. Physiol* 279 (1), R202–R209. 10.1152/ajpregu.2000.279.1.r202. [PubMed: 10896883]
- Stjernschantz J, Bill A, 1980. Vasomotor effects of facial nerve stimulation: noncholinergic vasodilation in the eye. *Acta Physiol. Scand* 109, 45–50. 10.1111/j.1748-1716.1980.tb06562.x. [PubMed: 7446161]
- Stone RA, Kuwayama Y, Laties AM, 1987. Regulatory peptides in the eye. *Experientia* 43, 791–800. 10.1007/BF01945357. [PubMed: 3297767]
- Ten Tusscher MPM, Klooster J, Baljet B, Van der Werf F, Vrensen GFJM, 1990. Pre- and post-ganglionic nerve fibres of the pterygopalatine ganglion and their allocation to the eyeball of rats. *Brain Res.* 517, 315–323. 10.1016/0006-8993(90)91043-G. [PubMed: 1695865]
- Told R, Palkovits S, Haslachner H, Frantal S, Schmidl D, Boltz A, Lasta M, Kaya S, Werkmeister RM, Garhöfer G, Schmetterer L, 2013. Alterations of choroidal blood flow regulation in young healthy

- subjects with complement factor H polymorphism. *PLoS One* 8 (4), e60424. 10.1371/journal.pone.0060424. [PubMed: 23596508]
- Tóth IE, Boldogkoi Z, Medveczky I, Palkovits M, 1999. Lacrimal preganglionic neurons form a subdivision of the superior salivatory nucleus of rat: transneuronal labelling by pseudorabies virus. *J. Auton. Nerv. Syst* 77, 45–54. 10.1016/S0165-1838(99)00032-6. [PubMed: 10494749]
- Tso MOM, Jampol LM, 1990. Hypertensive retinopathy, choroidopathy & optic neuropathy of hypertensive ocular disease. In: Laragh JH, Brenner BM (Eds.), *Hypertension: Pathophysiology, Diagnosis & Management*. Raven Press, New York, pp. 433–465.
- Tso MOM, 1988. Photic injury to the retina and pathogenesis of age-related macular degeneration. In: Tso MOM (Ed.), *Retinal Disease: Biomedical Foundations & Clinical Management*. Lippincott Co., Philadelphia, pp. 187–214.
- Von Leithner PL, Kam JH, Bainbridge J, Catchpole I, Gough G, Coffey P, Jeffery G, 2009. Complement factor H is critical in the maintenance of retinal perfusion. *Am. J. Pathol* 175, 412–421. 10.2353/ajpath.2009.080927. [PubMed: 19541934]
- Yancey CM, Linsenmeier RA, 1989. Oxygen distribution and consumption in the cat retina at increased intraocular pressure. *Invest. Ophthalmol. Vis. Sci* 30, 600–611. [PubMed: 2703301]
- Yancey CM, Linsenmeier RA, 1988. The electroretinogram and choroidal PO₂ in the cat during elevated intraocular pressure. *Invest. Ophthalmol. Vis. Sci* 29, 700–707.
- Zagvazdin YS, Fitzgerald MEC, Sancesario G, Reiner A, 1996a. Neural nitric oxide mediates Edinger-Westphal nucleus evoked increase in choroidal blood flow in the pigeon. *Invest. Ophthalmol. Vis. Sci* 37, 666–672. [PubMed: 8595967]
- Zagvazdin YS, Sancesario G, Wang YX, Share L, Fitzgerald MEC, Reiner A, 1996b. Evidence from its cardiovascular effects that 7-nitroindazole may inhibit endothelial nitric oxide synthase in vivo. *Eur. J. Pharmacol* 303, 61–69. 10.1016/0014-2999(96)00106-9. [PubMed: 8804912]
- Zhang HQ, Fast W, Marletta MA, Martasek P, Silverman RB, 1997. Potent and selective inhibition of neuronal nitric oxide synthase by N(ω)-propyl-L-arginine. *J. Med. Chem* 40, 3869–3870. 10.1021/jm970550g. [PubMed: 9397167]

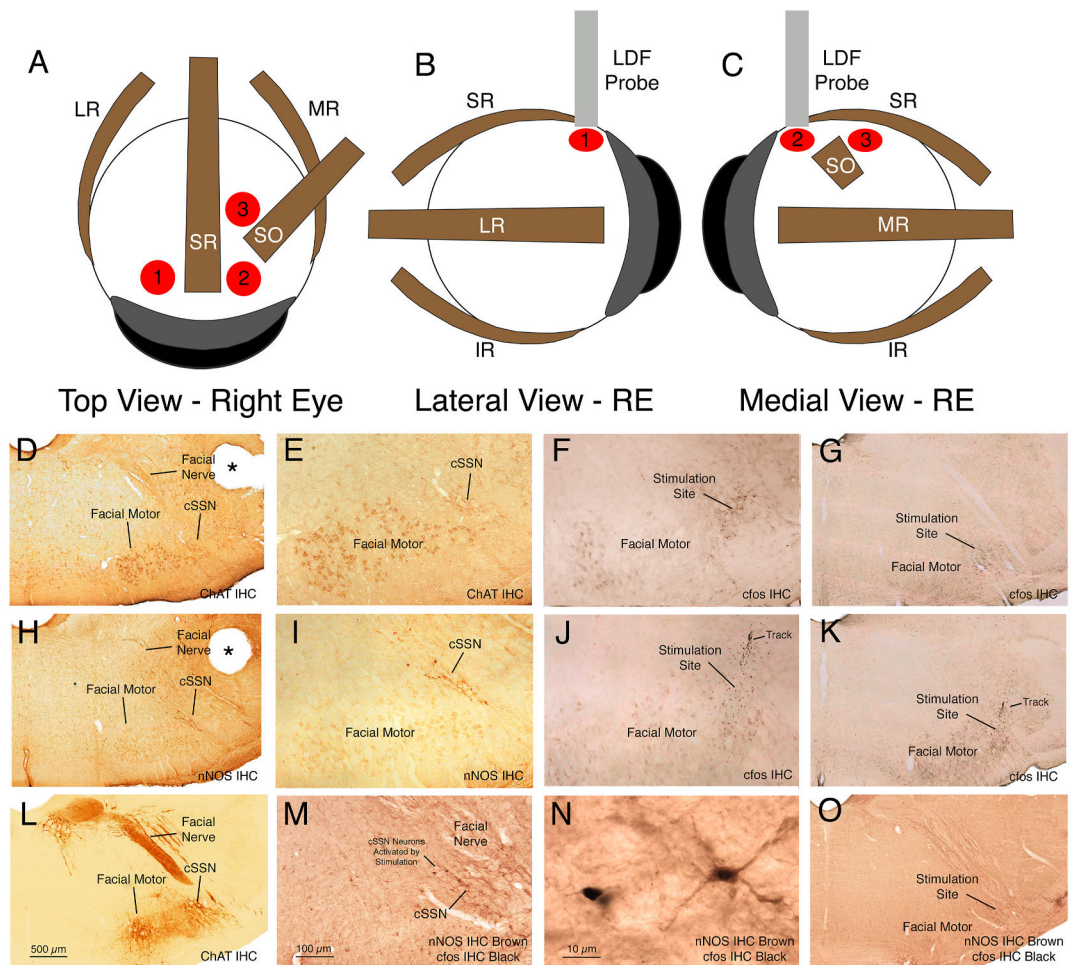


Fig. 1.

Panels A–C show schematics of the three ChBF recording sites for the right eye (RE), the anterior temporal site (1), the anterior nasal site (2), and the posterior nasal site (3), as seen in a dorsal view (A), lateral view (B), and medial view (C). Panels D–O show images of choroidal SSN just lateral to the facial motor nuclear complex, at a level corresponding to Paxinos and Watson (2009) –10.5 mm Bregma, in a ChAT-immunostained section at a low (D) and a high magnification (E), the stimulation site in choroidal SSN in rat RChBF52 as indicated by cfos+ neurons at the stimulation site at a high (F) and a low magnification (G), choroidal SSN just lateral to the facial motor nuclear complex in a nNOS-immunostained section at a low (H) and a high magnification (I), the stimulation site in choroidal SSN in rat RChBF53 as indicated by cfos+ neurons at the stimulation site (note electrode track at upper edge of the field of cfos+ neurons) at a high (J) and a low magnification (K), the level of the stimulation site in rostral choroidal SSN in rat RChBF29 in a ChAT-immunolabeled section at low magnification (L), the stimulation site in rostral choroidal SSN in rat RChBF29 at higher magnification as indicated by cfos in nNOS+ neurons of choroidal SSN (M), a higher magnification view of two cfos+/nNOS+ choroidal SSN neurons in RChBF29 (N), and the stimulation site in rostral choroidal SSN in rat RChBF29 as indicated by cfos in nNOS+ neurons of choroidal SSN at the same low magnification as shown in panel L (O). The ChAT

and nNOS immunolabeling was detected with a brown DAB reaction product, while cFos was detected with a black nickel-enhanced DAB reaction product. The scale bar in M pertains to E, F, I, and J as well, while that in L pertains to D, G, H, K and O as well. Abbreviations: ChAT – choline acetyltransferase; cSSN – choroidal subdivision of SSN; IHC – immunohistochemistry; IR – inferior rectus muscle; LR – lateral rectus muscle; MR – medial rectus muscle; nNOS – neuronal nitric oxide synthase; RE – right eye; SO – superior oblique muscle; SR – superior rectus muscle.

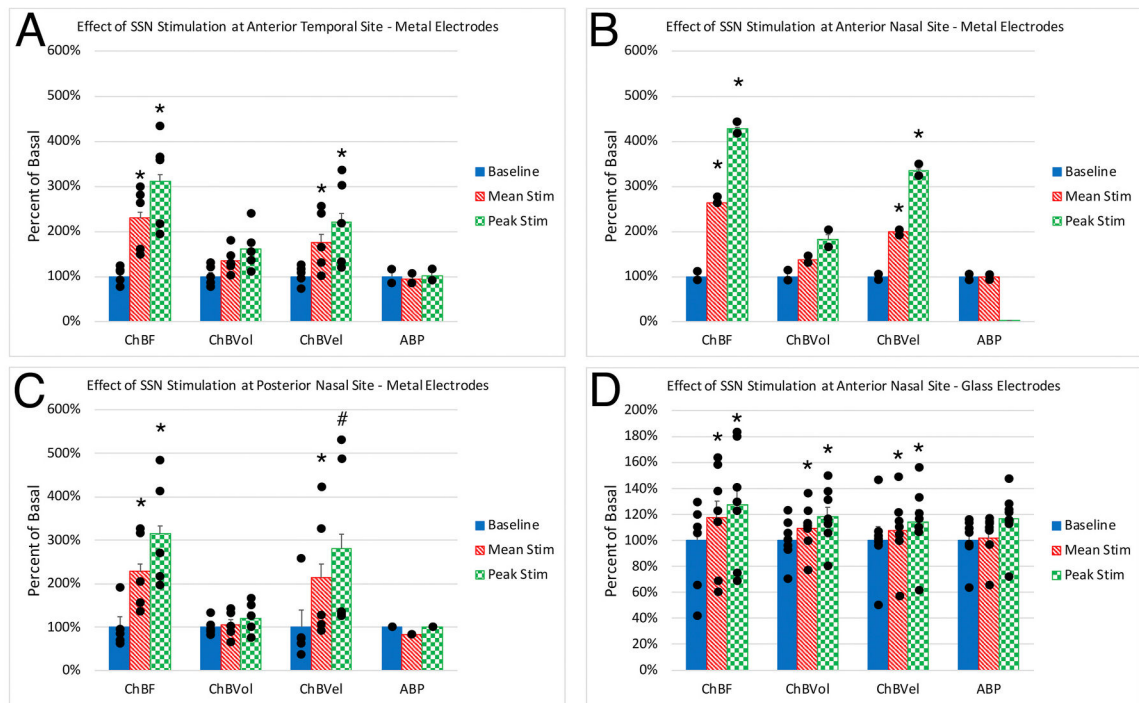


Fig. 2. Effect of choroidal SSN stimulation on ChBF, ChBVol, ChBVel, and ABP responses with metal electrodes at the anterior temporal (A, n = 5), anterior nasal (B, n = 2) and posterior nasal (C, n = 5) recording sites, and with glass micropipette electrodes at the anterior nasal site (D, n = 7). Stimulation yielded significant increases in mean and peak ChBF and ChBVel at all sites with metal electrodes, and ChBF, ChBVol, and ChBVel were all significantly increased at the anterior nasal site with glass micropipette electrodes. Asterisks indicate significantly different from baseline, and pound symbol indicates a trend toward significance.

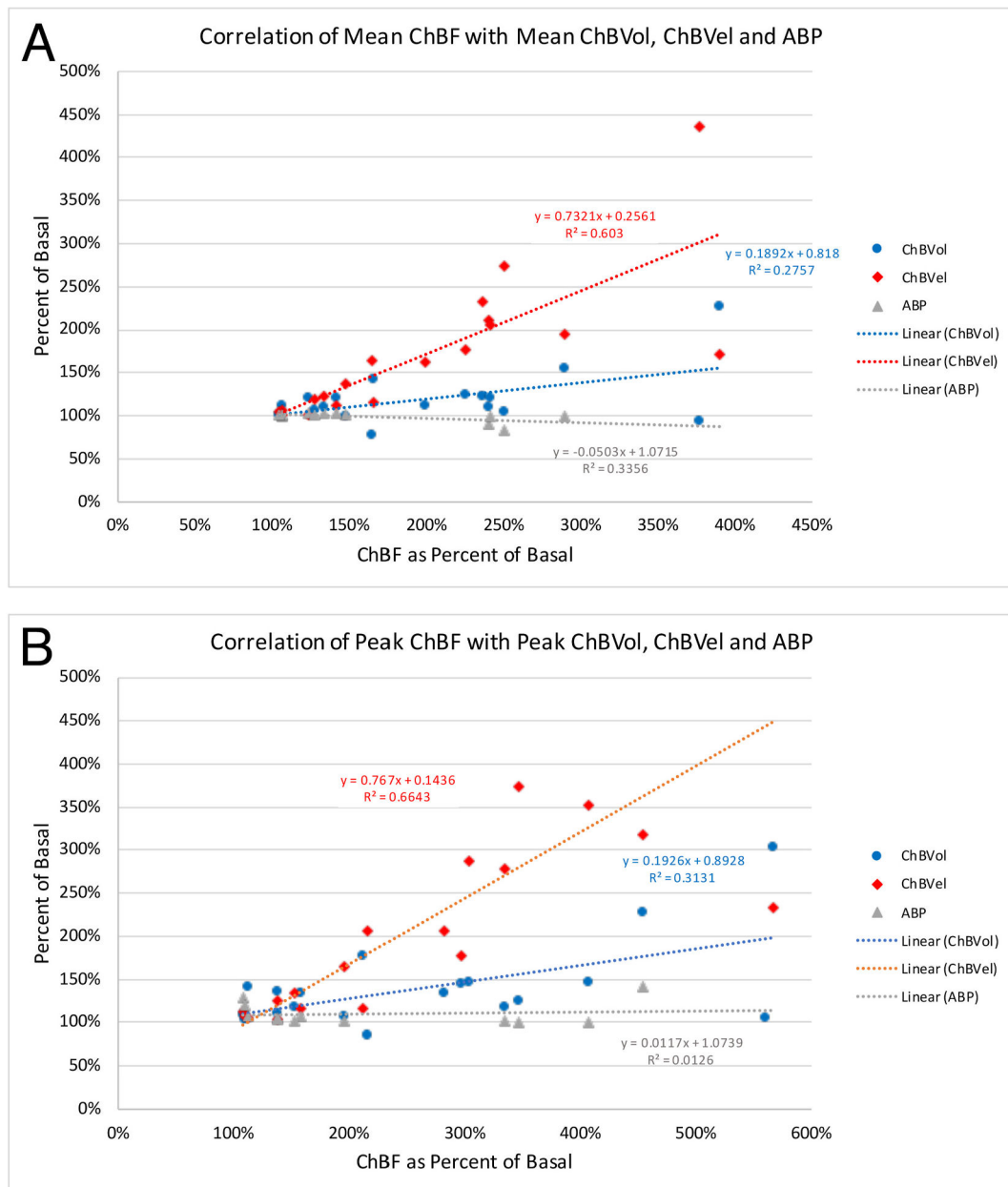


Fig. 3. Correlation of mean (A) and peak (B) ChBF with mean and peak ChBVol (blue regression line), ChBVel (red regression line), and ABP (grey regression line) across all animals and all recording sites ($n = 19$). The formula boxes show the slope and y-intercept for the regression lines, and the r^2 values for the regressions. Note that ChBVel is highly correlated with ChBF, ChBVol is less correlated with ChBF, and ABP is not correlated with ChBF.

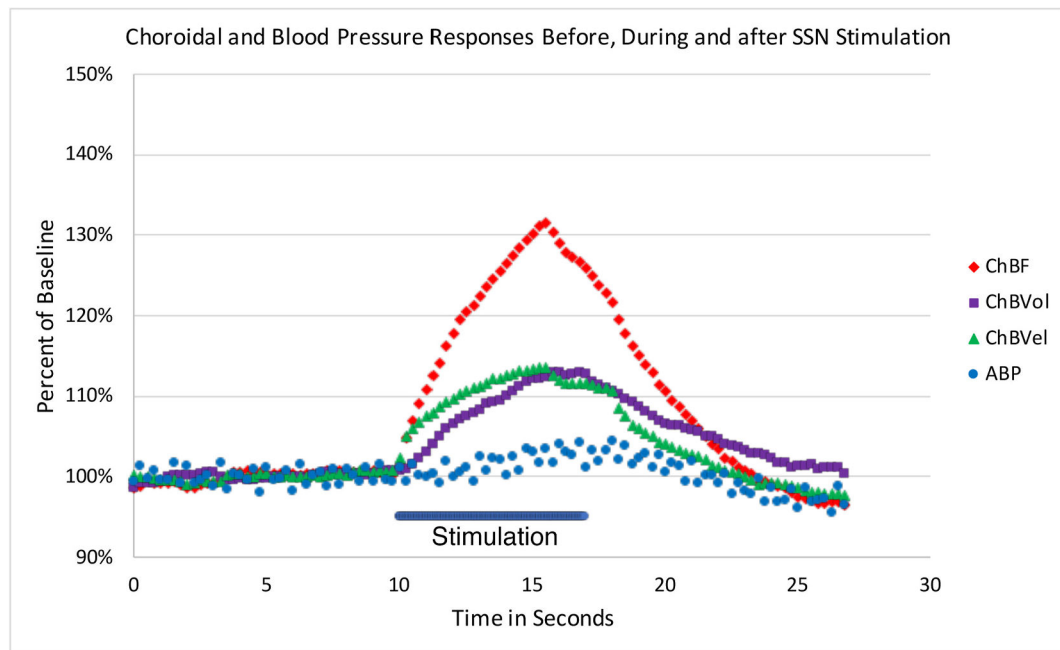


Fig. 4.

Graph showing the time course of the mean ChBF, ChBVol, ChBVel and ABP responses to choroidal SSN stimulation, for six of the rats with glass micropipette stimulation. The blue bar marks the stimulation period. Each data point is the mean for a 250 ms interval, and ChBF, ChBVol, ChBVel and ABP responses are all expressed as percent of basal. The rapid ChBF rise is driven by rapid increases in both choroidal blood velocity and volume, with the ChBVel rise being somewhat earlier than the ChBVol rise, consistent with our overall analysis showing a somewhat greater role of blood flow velocity increases in the ChBF increase.

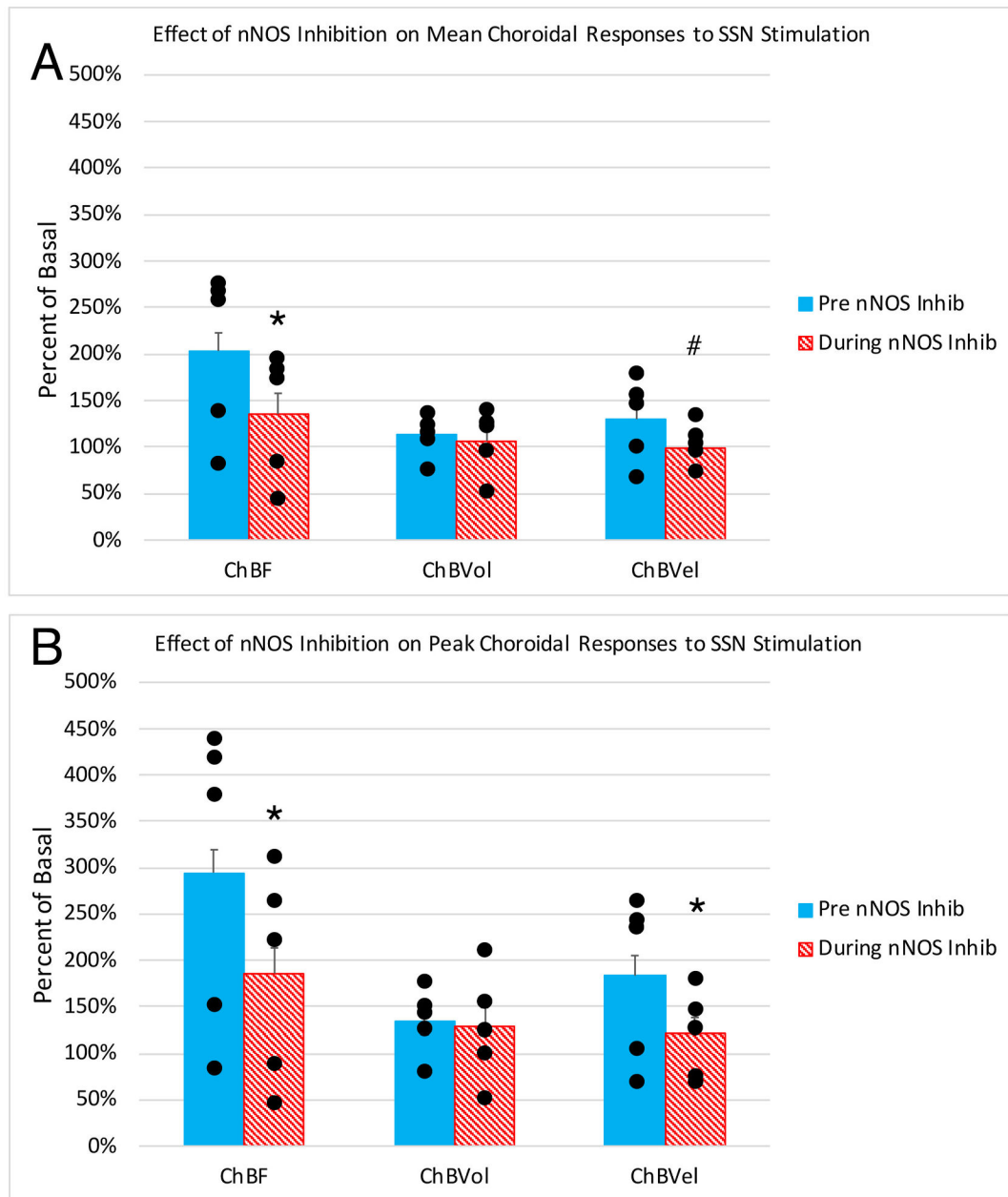


Fig. 5. Histograms showing the mean (A) and peak (B) ChBF, ChBVol and ChBVel responses to choroidal SSN stimulation, expressed as a percent of basal ChBF, ChBVol and ChBVel responses, prior to NOS inhibition and after NOS inhibition ($n = 5$). Note that SSN stimulation prior to NOS inhibition yielded significant ChBF, ChBVol and ChBVel increases, and that NOS inhibition attenuated the ChBF, ChBVol and ChBVel increases. Asterisks indicate significantly less than prior to NOS inhibition, pound symbol indicates a trend toward significance.

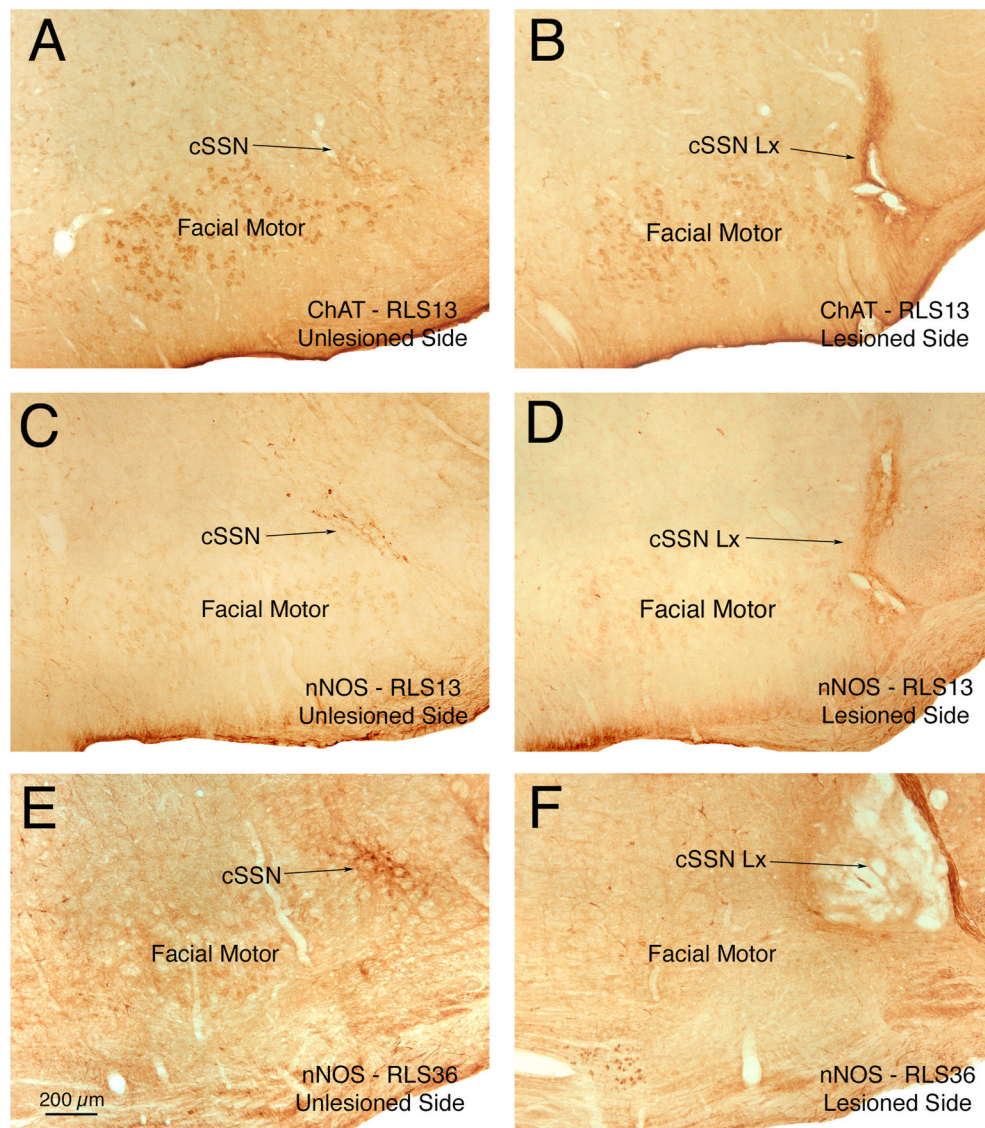
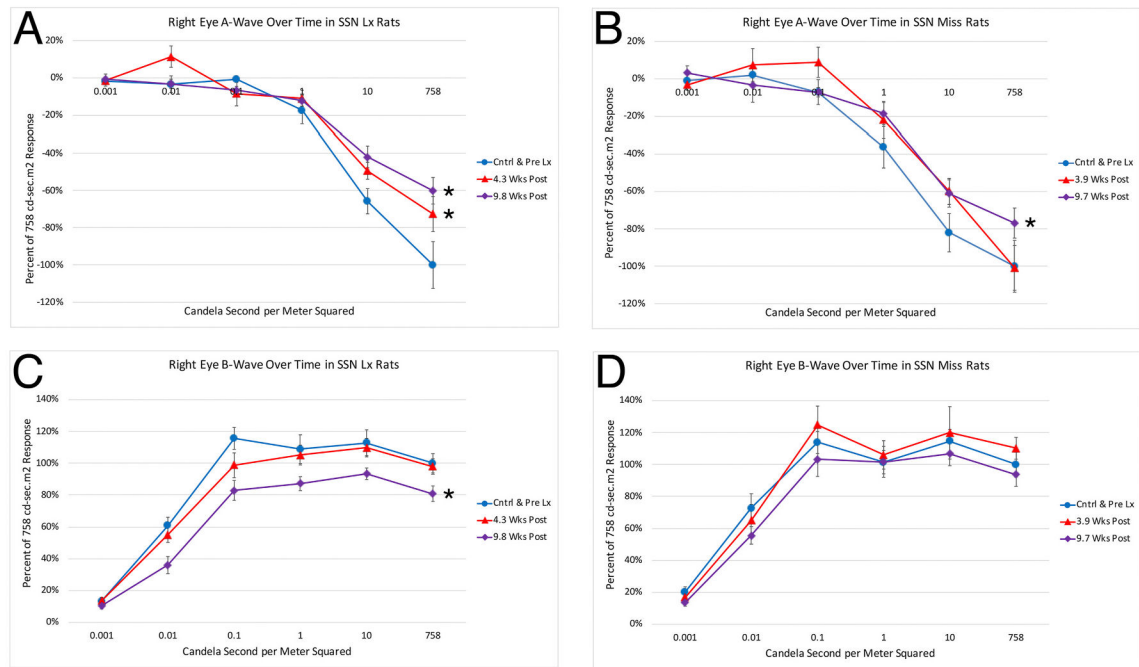
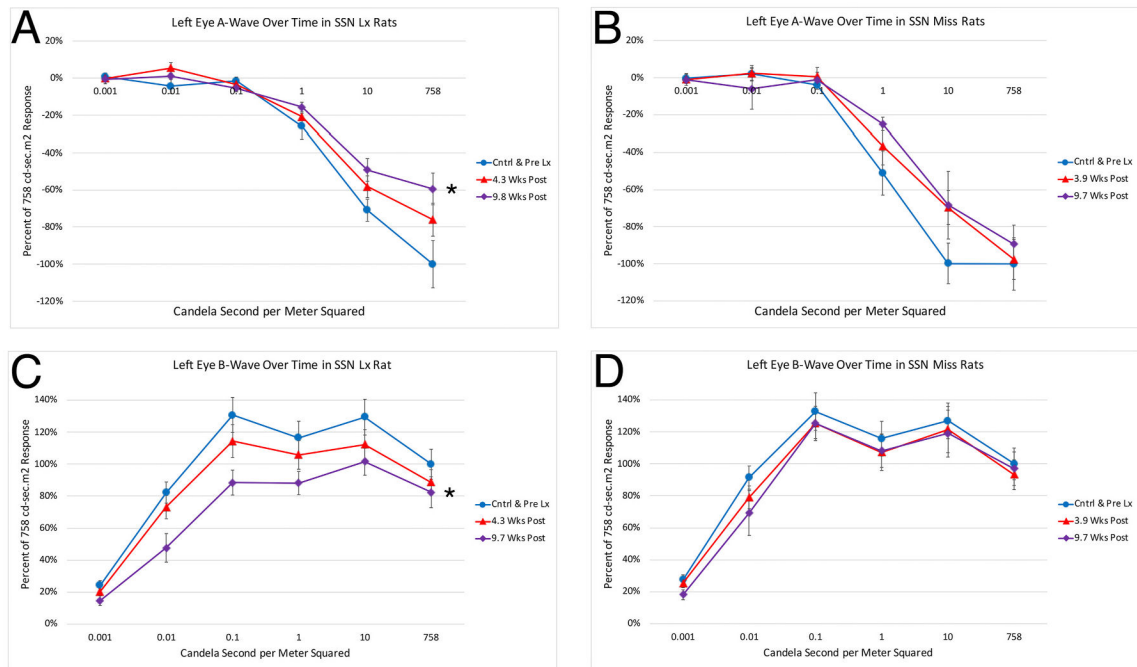


Fig. 6. Images showing right choroidal SSN in several rats, three to four months after an electrolytic lesion. Sections were immunolabeled for ChAT or nNOS, both of which are found in choroidal SSN neurons, to assess lesion accuracy. Successful (100%) destruction of right choroidal SSN is shown for rat RLS13 immunolabeled for ChAT (B) and nNOS (D) compared to choroidal SSN of the left side of its brain, and for right choroidal SSN for RLS36 immunolabeled for nNOS (F), compared to the left side of its brain (E). Left side images are flipped horizontally for ease of comparison to the right side. Abbreviations: ChAT – choline acetyltransferase; cSSN – choroidal subdivision of SSN; Lx – lesion; nNOS – neuronal nitric oxide synthase.

**Fig. 7.**

Graphs showing the mean flash-evoked scotopic a-wave peak amplitudes (A, B) and b-wave (C, D) peak amplitudes for the right eye in response to a series of light flashes, prelesion and at two different time points post lesion, for rats with lesions that destroyed right choroidal SSN (A, C) compared to rats with lesions that missed right choroidal SSN (B, D).

Amplitudes are expressed as a percent of the pre-lesion response to the brightest light flash to facilitate comparisons between rats with SSN destruction and rats without. **Panel A.** At 4 and 10 weeks post-lesion, a-wave peak was significantly reduced for the right eye in right SSN-Lx rats (n = 11) compared to prelesion (n = 10) for the three brightest light intensities (asterisks). **Panel B.** The a-wave peak of the right eye for the three brightest light intensities was not significantly reduced in right SSN-miss rats (n = 9) compared to prelesion (n = 9) at 4 weeks post lesion attempt, but it was at ten weeks (asterisk). **Panel C.** At 10 weeks post lesion, the b-wave peak was significantly reduced for the right eye in right SSN-Lx rats (n = 11) compared to prelesion (n = 10) for the five brightest light intensities (asterisk). **Panel D.** The b-wave peak was not significantly reduced for the right eye in right SSN-miss rats (n = 9) compared to prelesion (n = 9) for the five brightest light intensities at either 4 or 10 weeks post lesion attempt.

**Fig. 8.**

Graphs showing the mean flash-evoked scotopic a-wave (A, B) and b-wave (C, D) peak amplitudes for the left eye in response to a series of light flashes, prelesion and at two different time points post lesion, for rats with lesions that destroyed right choroidal SSN (A, C) compared to rats with lesions that missed right choroidal SSN (B, D). Amplitudes are expressed as a percent of the prelesion response to the brightest light flash to facilitate comparisons between rats with SSN destruction and rats without. **Panel A.** At 10 weeks post lesion, but not 4 weeks, the a-wave peak was significantly reduced for the left eye in right SSN-Lx rats (n = 11) compared to pre-lesion (n = 10) for the 3 brightest light intensities (asterisk). **Panel B.** At neither 4 nor 10 weeks post SSN-miss was the a-wave peak significantly reduced for the left eye in right SSN-miss rats (n = 9) compared to prelesion (n = 9) for the three brightest light intensities. **Panel C.** At 10 weeks but not 4 weeks post lesion, the b-wave peak was significantly reduced for the left eye in right SSN-Lx rats (n = 11) compared to prelesion (n = 10) for the five brightest light intensities (asterisk). **Panel D.** At neither 4 nor 10 weeks post SSN-miss was the b-wave peak significantly reduced for the left eye in right SSN-miss rats (n = 9) compared to prelesion (n = 9) for the five brightest light intensities.

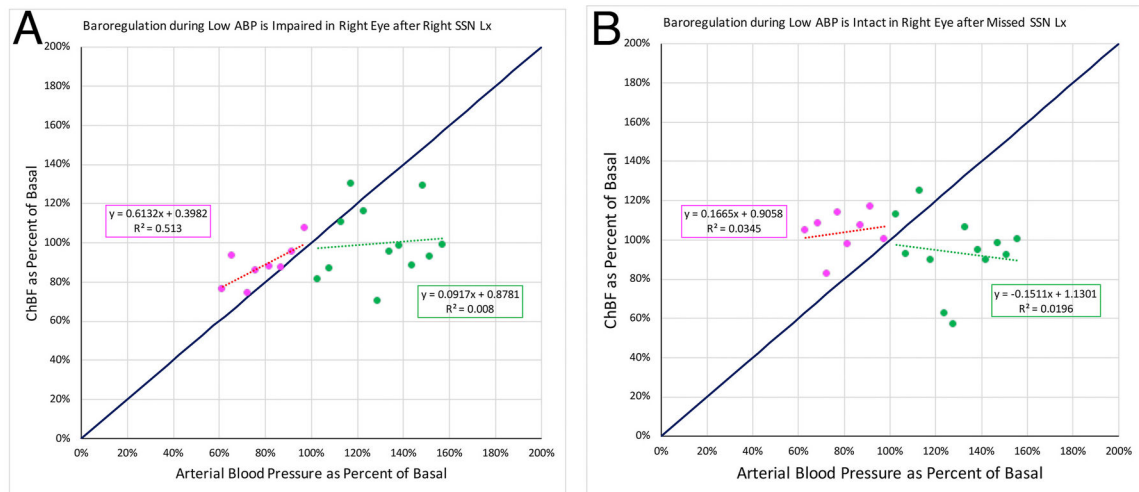


Fig. 9.

The graph shows ChBF plotted as a function of ABP for rat eyes ipsilateral to right choroidal SSN destruction (A, $n = 3$) compared to rats with lesions that missed right choroidal SSN (B, $n = 3$), with both ChBF and ABP expressed as a percent of basal. Mean ChBF performance is plotted per 5 mmHg ABP bin over a range of 40% below and 60% above basal ABP. The blue line shows ChBF as it would be if it linearly followed ABP. The formula boxes show the slope and y-intercept for the regression lines, and the r^2 value for the regressions. **Panel A.** The graph shows ChBF plotted as a function of ABP, in eyes ipsilateral to SSN-Lx. Note that ChBF during ABP <100% of basal changed nearly linearly with ABP. The magenta box shows that the slope of the ABP-ChBF relationship during low ABP approached 1, and their correlation was 0.716. ChBF remained relatively flat, however, at ABP greater than 100% of basal, the green box showing a flat slope and low correlation of the ABP-ChBF relationship. **Panel B.** The graph shows ChBF plotted as a function of ABP, in eyes ipsilateral to lesions that missed SSN. Note that ChBF during ABP <100% of basal changed little as ABP changed. The magenta box shows that the slope of the ABP-ChBF relationship during low ABP approached 0, and their correlation was also nearly 0. ChBF remained relatively flat also at ABP greater than 100% of basal, the green box showing a flat slope and low correlation of the ABP-ChBF relationship.

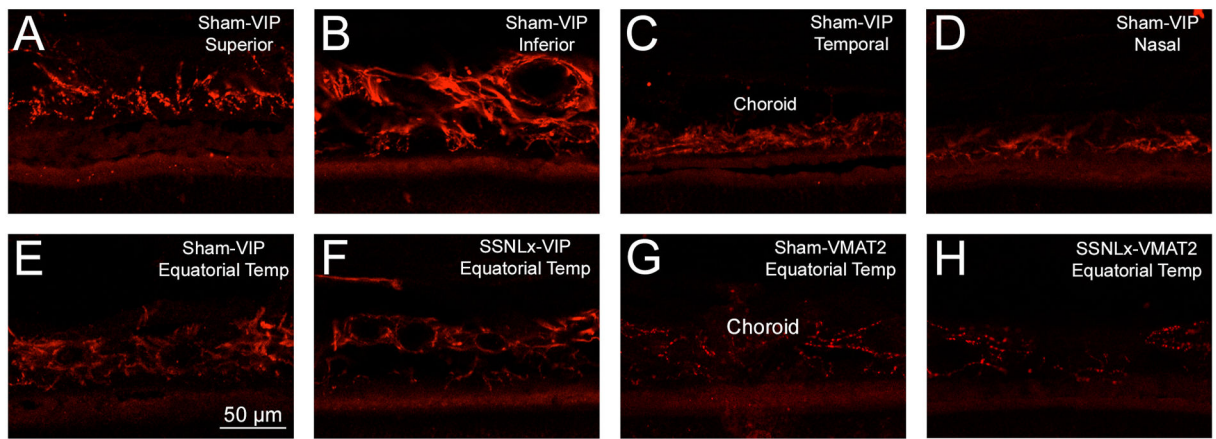


Fig. 10.

Images showing that VIP+ parasympathetic innervation is evident throughout choroid, as evidenced by the abundance of vascular innervation in the superior (A), inferior (B), temporal (C) and nasal (D) sectors of the eye. Moreover, neither the parasympathetic innervation nor sympathetic innervation is obviously affected by lesions of choroidal SSN, as evidenced by similar immunolabeling for VIP for equatorial temporal choroid ipsilateral to destruction of choroidal SSN (E) compared to contralateral to the lesion (F), and similar immunolabeling for VMAT2 in equatorial temporal choroid ipsilateral to destruction of choroidal SSN (G) compared to contralateral to the lesion (H).

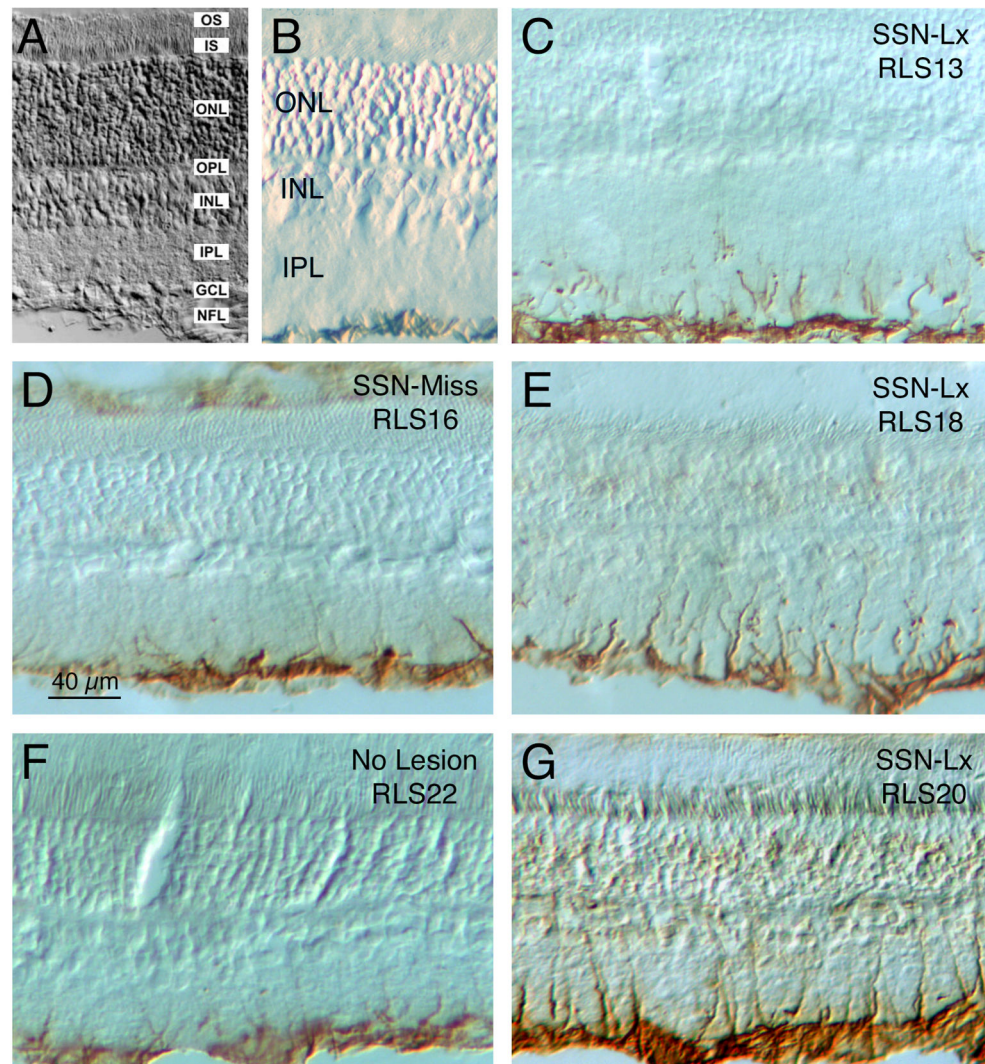


Fig. 11. Images showing the effects of destruction of choroidal SSN on GFAP immunolabeling of retinal Müller cell processes in the ipsilateral eye ~3 months post lesion. Images A and B show retinal layer organization, while images D and F show retina ipsilateral to a missed SSN lesion (D) or after no lesion (F), and images C, E, and G show retina ipsilateral to choroidal SSN destruction (cSSN-Lx). Note that in cSSN-Lx rats, intense GFAP immunolabeling was seen in Müller cell processes in the IPL of the ipsilateral eye (C, E, and G), but not in control retinas (D, F). GFAP upregulation occurred throughout the topographic extent of the retina (images show superior retina). Abbreviations: GCL – ganglion cell layer; INL – inner nuclear layer; IPL – inner plexiform layer; IS – inner segments; ONL – outer nuclear layer; OPL – outer plexiform layer; OS – outer segments; NFL – nerve fiber layer.

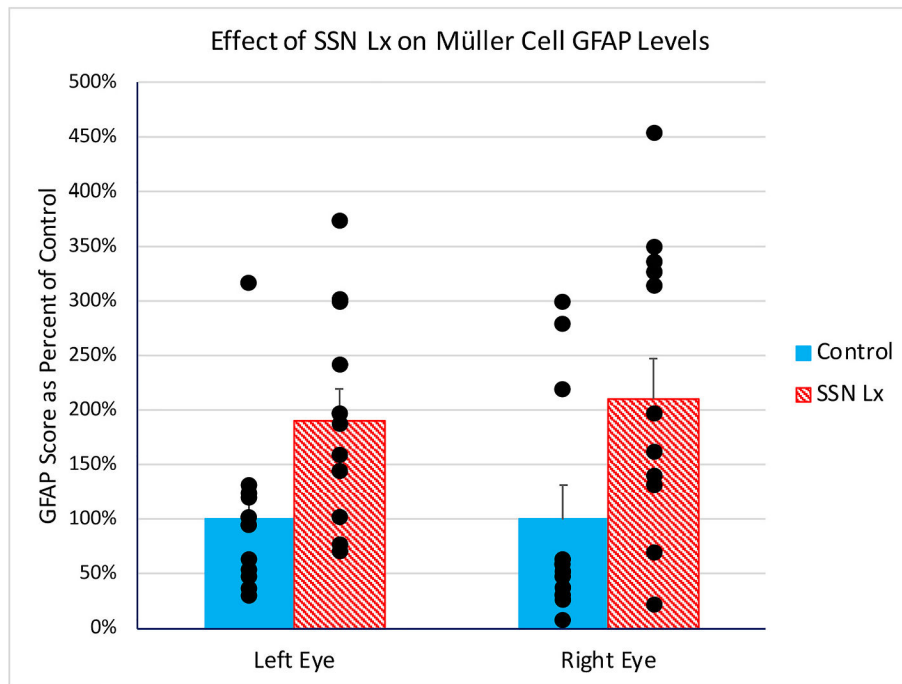


Fig. 12.

In rats with unilateral right destruction of choroidal SSN ($n = 12$), intense GFAP immunolabeling was seen in Müller cell processes in IPL in both eyes, but not in control retinas, which included SSN-miss cases and normal control rats ($n = 11$). Using a scoring system for the GFAP immunolabeling of Müller cell processes (Kimble et al., 2006), labeling in SSN-Lx retinas at a mean postlesion survival of 13.5 weeks was significantly elevated (asterisk) above that in control retinas with a mean post-lesion survival of 11.5 weeks for both eyes. Regression analysis showed the GFAP score was uncorrelated with survival across SSN-Lx and SSN-miss cases.

Table 1

Primers and Probes for TaqMan qPCR.

Target	Primer 1	Primer 2	Probe #
GFAP	tttccaacctccagatcc	tcttgaggtggcctctgac	64

Author Manuscript

Author Manuscript

Author Manuscript

Author Manuscript